IDENTIFICATION AND CHARACTERIZATION OF *Tmem16a* IN VERTEBRATE DEVELOPMENT

By

JASON RANDALL ROCK

A DISSERTATION PRESENTED TO THE GRADUATE SCHOOL
OF THE UNIVERSITY OF FLORIDA IN PARTIAL FULFILLMENT
OF THE REQUIREMENTS FOR THE DEGREE OF
DOCTOR OF PHILOSOPHY

UNIVERSITY OF FLORIDA

2008

To my parents and my sister

ACKNOWLEDGMENTS

I would like to thank my parents and my sister for their love and support without which I would have failed years ago. They have celebrated each of my life's successes and encouraged me through each of its challenges.

I am forever grateful to Dr. Brian Harfe for introducing me to the field of developmental genetics and for allowing me the freedom to explore many morphogenetic events firsthand. I appreciate his support and guidance as I dealt with each of this project's surprises. I would also like to thank my advisory committee members, Drs. Henry Baker, Martin Cohn, and Paul Oh, for their guidance.

A number of scientists have contributed to this work in many ways. Dr. Danielle Maatouk provided invaluable support and friendship. Dr. Amel Gritli-Linde was the source of countless transatlantic suggestions, criticisms, and protocols for which I am eternally grateful. Dr. Christopher Futtner performed the blastocyst injections without which much of this work would have been impossible. My labmates, Cort Bouldin and KyungSuk Choi, are thanked for their friendship, support, comments, and conversations. Drs. Karen Johnstone and Jim Resnick taught me the ways of the mouse embryonic stem cell and provided unimaginable support for a fledgling laboratory. For their technical contributions, I would like to thank Doug Smith and M. Cecilia Lopez.

I owe a great deal of gratitude to those who recognized and nurtured my scientific proclivity early in life. Notable among these individuals are Dr. Dexter Easton, Tess Durant, Otto Phanstiel, and Mark Landschoot.

Lastly, I would like to thank the people who have facilitated this work in the most practical sense. In particular, Joyce Conners, Michele Ramsey and Jenneene Spencer have made certain that I was well equipped and prepared for my graduate studies.

TABLE OF CONTENTS

page

LIST OF TABLES

LIST OF FIGURES

LIST OF ABBREVIATIONS

AER	apical ectodermal ridge
AMV	avian myelobastosis virus
BMP	bone morphogenetic protein
BSA	bovine serum albumin
cDNA	complimentary deoxyribonucleic acid
cRNA	complimentary ribonucleic acid
DNA	deoxyribonucleic acid
E	embryonic day
EDTA	ethylenediaminetetraacetic acid
ES	embryonic stem
EST	expressed sequence tag
FACS	fluorescence activated cell sorting
FGF	fibroblast growth factor
GFP	green fluorescent protein
GIST	gastrointestinal stromal tumor
HH	Hamburger and Hamilton chick stage
IVT	*in vitro* transcription
kb	kilobases
ng	nanogram
OSCC	oral squamous cell carcinoma
PBS	phosphate buffered saline
PCR	polymerase chain reaction
PFA	paraformaldehyde
RA	retinoic acid

RACE	rapid amplification of cDNA ends
RNA	ribonucleic acid
rpm	revolutions per minute
rRNA	ribosomal ribonucleic acid
rtPCR	reverse transcription polymerase chain reaction
SHH	sonic hedgehog
ug	microgram
ZPA	zone of polarizing activity

Abstract of Dissertation Presented to the Graduate School
of the University of Florida in Partial Fulfillment of the
Requirements for the Degree of Doctor of Philosophy

IDENTIFICATION AND CHARACTERIZATION OF *Tmem16a* IN VERTEBRATE DEVELOPMENT

By

Jason Randall Rock

May 2008

Chair: Brian D. Harfe
Major: Medical Sciences - Genetics

The development of a vertebrate embryo is a complex process that requires many precisely regulated morphogenetic events. For decades, scientists have studied vertebrate development in the context of the limbs because of their accessibility for manipulations and organisms' resistance to perturbations of limb development. Two signaling centers in the vertebrate limb, the zone of polarizing activity (ZPA) and the apical ectodermal ridge (AER), were identified by classical embryo manipulations. Such manipulations provide the context into which we incorporate molecular data.

It has been shown that the secreted molecule sonic hedgehog (SHH) mediates the polarizing activity of the ZPA in the limb. Deletion or misexpression of *Shh* results in severe patterning defects that recapitulate those observed in early embryological experiments. We are now beginning to understand the mechanisms by which SHH influences digit identity and limb outgrowth on a cellular level.

To identify additional genes expressed in the ZPA, we performed a microarray screen that compared the levels of over 39,000 transcripts between the ZPA and the rest of the limb bud. From this data, we confirmed the expression of six genes in the limb bud whose expression there

had not been previously reported. RNA *in situ* hybridization showed that at least four of these genes were expressed in the ZPA and might influence its function.

To investigate the function of one of these genes, *Tmem16a*, in vertebrate development, we generated a null allele of this gene in mouse embryonic stem cells. Mice homozygous for this allele do not have an apparent limb defect, but all homozygous mutants die within a month of birth. This demonstrates a requirement for *Tmem16a* in vertebrate development.

The epithelium of the mid-gestational trachea is stratified, or multi-layered, during normal mouse development. The molecular events responsible for this stratification are currently poorly understood. We report that the epithelium of *Tmem16a* mutant tracheae fails to stratify and the resulting lateral arrangement of epithelial cells causes an expansion of the tracheal tube. This expansion redirects the formation of cartilage in the surrounding mesenchyme so that multiple disconnected cartilage elements form instead of C-shaped rings that keep the trachea open during respiration.

Tmem16a is a member of a family of genes that comprises at least ten members in mice and humans. In support of our observation of an abnormal epithelial organization of *Tmem16a* mutant tracheae, two other members from this protein family have been shown to influence cellular morphology. In an attempt to better understand the functions of these proteins in vertebrate development, we have examined the *in vivo* expression patterns of *Tmem16a* and several other members of this family during mouse development. The expression of these genes is widespread during embryogenesis and, as we show for *Tmem16a* and *Tmem16f*, overlapping in a variety of tissues. The mutation of at least one member, *TMEM16E*, has been linked to the human disease gnathodiaphyseal dysplasia and the clinical relevance of this family is underscored by the expression of several *TMEM16*s in multiple types of cancer.

CHAPTER 1
INTRODUCTION

Limb Development

For decades scientists have investigated the complex mechanisms that regulate the development of the vertebrate limb. In a fortuitous experiment, John Saunders and Mary Gasseling grafted a population of mesenchymal cells from the posterior of one chick limb bud to the anterior of a recipient chick limb bud (Saunders JW and Gasseling, MT. 1968). This manipulation resulted in supernumerary digits that were patterned so that those closest to the anterior site of the graft assumed a more posterior identity. In this manner, the zone of polarizing activity, or ZPA, was identified as a signaling center that is necessary for the normal anteroposterior patterning of the vertebrate limb.

The ZPA was hypothesized to function by secreting a morphogen that established a gradient along the anteroposterior axis with different concentrations of the unidentified morphogen specifying digit identities (Wolpert, 1969). It was later discovered that retinoic acid (RA) was capable of inducing mirror-image duplications (Tickle et al., 1982) and that these duplications were dose-dependant (Tickle et al., 1985). However, the concentration of RA necessary to induce and pattern ectopic digits elicited responses in the anterior of the limb that were not observed in the endogenous ZPA (Noji et al., 1991). Careful study demonstrated that RA functions upstream of the ZPA (Wanek et al., 1991) but does not directly polarize the limb.

Sonic hedgehog, a homolog of *Drosophila* hedgehog, was identified as the ZPA morphogen (Riddle et al., 1993). *Shh* expression in the limb is confined to the domain shown to possess polarizing activity in ZPA grafting experiments. Furthermore, when fibroblasts expressing *Shh* were transplanted to the anterior of the limb, mirror-image duplications reminiscent of those seen in ZPA grafts were observed. Genetic knockout in mice demonstrated

that SHH functions not only to pattern the anteroposterior axis of the limb bud, but also plays a role in regulating the outgrowth of the limb (Chiang et al., 1996).

In addition to the ZPA, a second signaling center, the apical ectodermal ridge (AER), is necessary for the outgrowth of the limb (Saunders JW, 1948). Fibroblast growth factors (FGFs) expressed in the AER are necessary for the maintenance of *Shh* expression in the ZPA (Niswander et al., 1994). Conversely, SHH in the ZPA is capable of regulating *Fgf4* expression and functions in a positive feedback loop that promotes the outgrowth of the limb (Laufer et al., 1994; Niswander et al., 1994). The bone morphogenetic protein (BMP) antagonist gremlin is induced in the limb bud mesenchyme in response to low levels of BMP2 (Nissim et al., 2006) and prevents the *Bmp*-mediated regression of the AER (Ganan et al., 1998). It has recently been shown that descendants of *Shh*-expressing cells do not express gremlin (Scherz et al., 2004). As the limb bud grows, a wedge of gremlin-negative cells forms between the *Shh*-expressing cells of the ZPA and the *Fgf*-expressing cells of the AER. This results in the eventual breakdown of the *Shh*-*Fgf* feedback loop and the termination of limb outgrowth.

By irreversibly marking the descendants of *Shh*-expressing cells using the *Shhgfpcre* allele (Harfe et al., 2004) and a lacZ reporter allele (Soriano, 1999), we have previously shown that the most posterior digits arise from cells that expressed *Shh* in the ZPA (Harfe et al., 2004). The identities of digit 4 and digit 5, which are completely derived from cells that have expressed *Shh*, are specified by the duration of their exposure to SHH. Cells giving rise to digit 5 are exposed to high concentrations of SHH for a longer period of time than those giving rise to digit 4. In contrast, specification of digit 2 is determined only by the concentration of SHH that has diffused across the limb field. Digit 3 is composed of a mixture of cells, some of which have actively expressed *Shh* and some that have only responded to SHH protein (Harfe et al., 2004).

Consistent with the data from *Shh* null mice (Chiang et al., 1996), digit 1 specification is *Shh*-independent.

Identifying Additional Genes Expressed During Mouse Limb Development

To date, *Shh* is the only gene known to be specifically expressed in the ZPA of the vertebrate limb. Initially, this work focuses on the identification of other genes expressed in the ZPA. These factors might be involved in the secretion or reception of SHH, serve as a cellular memory of previous exposure to SHH, regulate proliferation and/or differentiation in the limb or function in other unforeseen pathways.

To identify additional genes expressed in the ZPA, we used the *Shhgfpcre* allele (Harfe et al., 2004) in combination with fluorescence-activated cell sorting (FACS) to purify two populations of cells from the mouse limb: one from the ZPA and one from the rest of the limb bud. From these populations, labeled cRNA was synthesized and hybridized to Affymetrix GeneChips to identify genes differentially expressed between the ZPA and the rest of the limb. Analysis of the microarray data identified a number of genes that might have higher levels of expression in the ZPA compared to the rest of the limb bud. From this list, we confirmed the expression of six genes with previously unidentified expression in the mouse limb bud (Rock et al., 2007).

The Role of *TMEM16A* in Vertebrate Development

One of the genes identified by this screen, *Tmem16a,* is a member of the evolutionarily conserved TMEM16 family of genes. The human ortholog, *TMEM16A* (other published names for this gene include *TAOS2*, *FLJ10261*, *DOG1*), is overexpressed in a variety of cancers including gastrointestinal stromal tumors (GISTs) and oral squamous cell carcinomas (OSCCs) (West et al., 2004) (Huang et al., 2006). The mouse ortholog of *Tmem16a* was identified on chromosome 7, but had not previously been characterized *in vivo* (Katoh and Katoh, 2003).

We took a reverse genetics approach to elucidate the normal function of *Tmem16a* in vertebrate development by generating a null mouse allele in embryonic stem (ES) cells. All mice homozygous for this mutation die within one month of birth suggesting that *Tmem16a* is essential for normal development. Widespread embryonic expression of *Tmem16a* implies that a number of developmental processes might not occur normally in *Tmem16a* mutants; however, we focused on characterizing one defect in mice homozygous for this allele.

C-shaped rings of hyaline cartilage normally surround the trachea and prevent its collapse during respiration. Reverse genetic experiments in mice have demonstrated the involvement of several molecules in the development of the cartilage rings including *Shh* (Miller et al., 2004), *Traf4* (Regnier et al., 2002), *FoxF1* (Mahlapuu et al., 2001) and retinoic acid (Mendelsohn et al., 1994; Vermot et al., 2003). Tracheal cartilage defects in these models are accompanied by other defects and have not been investigated in detail. Therefore, the embryology of the tracheal cartilage is not well understood. We found that all *Tmem16a* mutant mice exhibit a severe disruption in the normal pattern of the cartilage rings that extends the entire length of the trachea. Careful examination revealed that this disruption occurs as the result of a mechanical force exerted on the developing cartilage condensations from the tracheal epithelium that they encircle.

In normal mouse development, the cells of the embryonic tracheal epithelium undergo stratification so that the epithelium is 2-3 cell layers thick at E15.5 (Daniely et al., 2004). In *Tmem16a* mutants, the epithelium does not stratify properly and is instead only 1-2 cell layers thick. One consequence of this stratification defect is that the diameter of the tracheal tube is expanded and the epithelium evaginates into the surrounding mesenchyme. The aberrant epithelial evagination in *Tmem16a* mutants divides the normal ventrolateral population of

chondrocytes into discontinuous populations that contribute to disrupted cartilage elements instead of rings.

The TMEM16 Family of Proteins

A single TMEM16 homolog, IST2, is found in the genome of the budding yeast *Saccharomyces cerevisiae*. This protein has been found to sort asymmetrically during cell division and has been implicated in maintaining osmotic homeostasis (Takizawa et al., 2000) (Entian et al., 1999). There exist in mice and humans 10 paralogs in the TMEM16 family of proteins (Katoh and Katoh, 2005) (Mizuta et al., 2007). Very little data concerning the *in vivo* expression patterns and functions for these genes has been reported.

We have investigated in detail the expression pattern of *Tmem16a* during vertebrate development. We report that *Tmem16a* is expressed in tissues derived from all three germ layers. Examples of mesoderm-derived tissues that express Tmem16a are the trachealis muscle dorsal to the trachea and the ZPA in the limb. Endoderm-dervived tissues that express *Tmem16a* include the epithelia of the trachea and lung. We also detected expression of *Tmem16a* in ectodermal derivatives including the skin and sensory epithelia of the retina, inner ear, and olfactory epithelium. *Tmem16a* is expressed in a number of branched organs including the lung, submandibular salivary glands and lacrimal glands.

A second signaling center in the limb bud, the apical ectodermal ridge, secretes members of the fibroblast growth factor family of proteins and is essential for outgrowth of the limb (Sun et al., 2002). We detected expression of a TMEM16 family member, *Tmem16c*, specifically in the AER of the mouse limb.

Gene trapped alleles are randomly generated insertions of a selection cassette into the genome. We identified and obtained a gene trapped allele of *Tmem16f*, a paralog of *Tmem16a*. We generated mice heterozygous for this allele, *Tmem16f*^{RRF355}/+, and used expression of the β-

geo reporter construct under the control of the endogenous *Tmem16f* regulatory elements to indirectly visualize expression of *Tmem16f* during mouse development. We observed β-galactosidase activity (and presumably expression of *Tmem16f*) in bones developing via both intramembranous and endochondral ossification. We also performed RNA *in situ* hybridization to detect *Tmem16f* in a variety of embryonic tissues, many of which overlapped with sites of *Tmem16a* expression.

The expression of members of the TMEM16 family of proteins is widespread during vertebrate development. In addition, orthologs of this family are conserved in organisms ranging from *S. cerevisiae* to humans. Together with the perinatal lethality observed in our *Tmem16a* mutants, this is strong evidence that members of this family are essential to the development of a variety of structures during embryogenesis. We have shown that *Tmem16a* might have a function in regulating cell morphology or cell:cell contacts in the embryonic tracheal epithelium and two other family members, *Tmem16e* and *Tmem16g*, have been shown to influence cellular morphology as well (Tsutsumi et al., 2004) (Das et al., 2007).

CHAPTER 2
IDENTIFICATION OF GENES EXPRESSED IN THE MOUSE LIMB USING A NOVEL ZPA MICROARRAY APPROACH

One well-studied signaling center in the developing vertebrate limb, the zone of polarizing activity (ZPA), produces the morphogen sonic hedgehog (*Shh*) that is necessary for normal growth and pattern formation. To identify additional factors expressed in the ZPA of the mouse limb bud, the *Shhgfpcre* allele was used to purify ZPA cells using fluorescence-activated cell sorting. Microarray technology was then used to identify genes whose expression was elevated in the ZPA compared to the rest of the limb. RNA *in situ* hybridization confirmed the expression of two known transcription factors, *Hlxb9* and *Tcfap2b*, an uncharacterized EST, and a transmembrane protein of unknown function in domains overlapping the ZPA. The expression of two other genes was confirmed by rtPCR.

An *in vivo* Screen to Identify Genes Expressed in the Mouse ZPA

To purify ZPA cells from the limb, limb buds were dissected from *Shhgfpcre*-heterozygous embryos (Figure 2-1). Mice heterozygous for this allele appear wild type and express green fluorescent protein (GFP) as well as the bacterial recombinase Cre in all cells that express *Shh* (Harfe et al., 2004). After dissociating the limbs into single cells, GFP-positive cells (the ZPA) and GFP-negative cells (the rest of the limb) were purified using fluorescence-activated cell sorting (FACS). Biotin-labeled cRNA was synthesized from each population of cells and hybridized to Affymetrix GeneChips. Analysis of the microarray data identified a number of genes that were differentially expressed in the ZPA and the rest of the limb (Table 2-1, Table 2-2, and data not shown). The raw data is available from the Gene Expression Omnibus of the National Center for Biotechnology Information (http://www.ncbi.nlm.nih.gov/geo/ accession number GSE7598).

Since our screen was designed to identify genes whose expression was enriched in the ZPA, we expected that *Shh* would be detected at higher levels in the GFP-positive cells. Indeed, this was the case; our array data indicated that *Shh* transcripts were more than 20 times as abundant in the ZPA cells than in the rest of the limb (Table 2-2). Other genes previously described as being present in the ZPA were also identified by our screen. For example, *Gli1*, *Bmp2* and *Hand2* were all detected at higher levels in the ZPA than in the rest of the limb. Our microarray data analysis of genes previously described as being expressed in the ZPA is summarized in Table 2-2. The identification of these genes suggested that our ZPA array screen might be capable of identifying novel genes expressed in this specific region of the limb bud.

In vivo Validation of Novel Genes Identified in the ZPA

To confirm *in vivo* that genes identified in our ZPA array screen were expressed in the limb bud, we performed whole mount RNA *in situ* hybridization for nine genes from our list of potential ZPA-specific genes (Table 2-1). None of these genes had been previously described in the embryonic day (E) 10.5 limb bud. Whole mount RNA *in situ* hybridization confirmed that four of these nine genes were expressed in domains overlapping the ZPA (Figure 2-2). For three of these genes, RNA *in situ* hybridization did not detect expression in the limb bud at E10.5, the stage at which the ZPA screen was performed (Figure 2-2F,J,N). Instead, for these genes, expression was first detected at E11.5 (Figure 2-2G,K,O). It is possible that these genes were expressed in the ZPA at E10.5 but were present below the level of detection of RNA *in situ* hybridization. A second possibility was that some of the embryos pooled to generate cRNA might have been slightly older than E10.5 (see Experimental Procedures).

Of the nine potentially ZPA-enriched genes for which we performed whole mount RNA *in situ* hybridization, we were unable to detect the expression of five in the limb bud. One explanation is that these genes were expressed in the limb bud, but present at levels below the

detection limit of RNA *in situ* hybridization. It was also possible that these five genes were false positives. To determine if these genes were expressed in the limb bud, we performed rtPCR using RNA isolated from E10.5 forelimbs as starting material. For two of these five genes, *Ppp1cb* and *Ywhaz*, we detected transcription in the E10.5 limb bud (Table 2-1).

Identification of Genes Expressed Outside the ZPA in the E10.5 Mouse Limb Bud

In addition to identifying genes expressed at elevated levels within the ZPA, the ZPA screen also identified genes expressed at higher levels outside of the ZPA. This list of genes contained some genes that had been previously characterized in the limb bud, for example gremlin (Zuniga et al., 1999), netrin (Puschel, 1999) and *Sox9* (Asou et al., 2002) (Table 2-2), as well as genes that were not previously described in the E10.5 limb bud (Table 2-1 and data not shown). We confirmed by RNA *in situ* hybridization the expression of netrin and an EST selected at random from this class of genes (EST BF583715; Figure 2-3A,B). In this report, we have focused on characterizing genes expressed in the ZPA. Our raw data, describing the entire transcriptome of the E10.5 mouse limb bud, has been made available from the Gene Expression Omnibus of the National Center for Biotechnology Information (http://www.ncbi.nlm.nih.gov/geo/ accession number GSE7598).

Genes with Expression in the ZPA

Tcfap2b

Analysis of the expression data indicated that the gene *Tcfap2b* was expressed at levels nearly four times higher in the ZPA than in the rest of the limb (Table 2-1). *Tcfap2b* encodes a member of the AP-2 family of transcription factors (Moser et al., 1997b) and had not previously been described in the limb. To confirm that the expression of this gene was elevated in the ZPA, we performed whole mount RNA *in situ* hybridization with an antisense probe homologous to the 3' end of the *Tcfap2b* transcript. Using this approach we first detected *Tcfap2b* transcripts in

the distal posterior of the limb bud at E11.5 in a region that overlapped the ZPA (Figure 2-2G). The domain of *Tcfap2b* expression at E11.5 extended much more anteriorly than that of *Shh* in the distal mensenchyme of the limb bud. Transcription of *Tcfap2b* continued until E12.5 with expression restricted to a very narrow posterior domain immediately adjacent to the overlying ectoderm (Figure 2-2H). At this later stage (E12.5), *Shh* is no longer expressed in the limb (Figure 2-2D).

Mice homozygous for a null allele of *Tcfap2b* have been generated. *Tcfap2b* homozygotes do not exhibit limb defects but die shortly after birth with polycystic kidney disease (Moser et al., 1997a).

Hlxb9

The gene *Hlxb9* encodes the homeodomain protein HB9. Transcription factors belonging to this family have a conserved DNA binding domain and are involved in the regulation of many genes that control a number of cellular functions (Cillo et al., 2001). Homeodomain transcription factors have been well studied in normal development and in disease (reviewed in (Manak and Scott, 1994; Samuel and Naora, 2005)). HB9 has been shown to play essential roles in mouse pancreatic development (Harrison et al., 1999) and the establishment of motor neuron identity (Thaler et al., 1999). In our screen, *Hlxb9* transcripts were detected at levels four times greater in the ZPA than in the rest of the limb (Table 2-1). *Hlxb9* expression had not previously been reported during any stage of limb development. To confirm that *Hlxb9* was expressed in the ZPA, we performed whole mount RNA *in situ* hybridization using an antisense probe with homology to the 5' end of the *Hlxb9* transcript. RNA *in situ* hybridization confirmed that *Hlxb9* expression was restricted to the posterior of the limb at E11.5 in a domain indistinguishable from that of *Shh* (Figure 2-2K). Hlxb9 transcripts were not detected in the limb bud before (E10.5) or after (E12.5) by RNA *in situ* hybridization (Figure 2-2J,L).

A targeted deletion of *Hlxb9* in mouse embryonic stem cells has been generated (Thaler et al., 1999). Mice homozygous for this deletion are smaller than littermates, have a "curled appearance," and die at birth of respiratory failure due to improper motor neuron specification (Thaler et al., 1999). These mice also exhibit defects in pancreatic development, but have no reported limb abnormalities (Harrison et al., 1999; Thaler et al., 1999).

In both mice and humans, *Hlxb9* is located about 100kb upstream of *Lmbr1*. Intron 5 of *Lmbr1* contains an enhancer element that is responsible for driving expression of *Shh* in the ZPA (Lettice et al., 2003). It is not known if this enhancer is also responsible for *Hlxb9* expression in the ZPA.

EST BI734849

A number of previously uncharacterized mouse expressed sequence tags (ESTs) were identified in our ZPA array screen. One of these, BI734849, was detected by RNA *in situ* hybridization at E11.5 in a narrow region of the posterior limb mesenchyme (Figure 2-2O). This expression domain did not extend to the anterior limit of the ZPA. An EST that partially overlapped with BI734849 but extended further 5' (AI853140) showed identical expression to BI734849 at E11.5 (data not shown). Expression of both ESTs persisted until E12.5 in a small domain in the proximal posterior of the developing autopod (Figure 2-2P). Although no protein product is reported from this locus, *in silico* translation yielded a protein with weak similarity to murine axonemal dynein heavy chains (~65% conservation across 60 amino acids). The syntenic locus in humans encodes the putative non-coding RNA NCRMS (Chan et al., 2002). In addition, we have found that the microRNA miR-135-a2 lies within an intron of this transcript. Whether or not miR-135a-2 is expressed in the ZPA remains to be determined.

Tmem16a

Tmem16a encodes one member of a recently identified family of eight-pass transmembrane proteins (reviewed in (Galindo and Vacquier, 2005)). In addition to the nine reported members of this protein family, *Tmem16a-Tmem16h* and *Trp53i5* (Katoh and Katoh, 2005), we have noted the existence of a tenth family member, *Tmem16k* (NM_133979). Although the TMEM16 family is highly conserved with homologs found in organisms ranging from *S. cerevisiae* to humans, the cellular functions of the 10 mammalian TMEM16 proteins are not known in any species.

In our ZPA screen, *Tmem16a* transcript levels were elevated 40 times higher in the ZPA than in the rest of the limb (Table 2-1). Whole mount RNA *in situ* hybridization confirmed that *Tmem16a* was expressed in the posterior fore- and hindlimb mesenchyme at E10.5 and E11.5 (Figure 2-2R,S). The expression domains of *Tmem16a* and *Shh* partially overlapped at these stages in the limb bud, but *Tmem16a* expression was restricted to a more proximal and posterior domain than *Shh*. *Tmem16a* expression was not observed at E9.5 in the limb (when *Shh* is first detected) or at E12.5 (Figure 2-2Q,T). In addition to *Tmem16a* expression in the posterior limb bud mesenchyme, RNA *in situ* hybridization detected Tmem16a expression in a variety of embryonic structures (see Chapters 3, 4, and 5).

Since TMEM16A is highly conserved at the protein level across species, it was of interest to determine if its expression pattern was also conserved. A search of the chicken EST database for *Tmem16a* indicated that there was an ortholog of this gene in chickens. RNA *in situ* hybridization using a *cTmem16a* probe indicated that, similarly to the expression pattern in mice, *cTmem16a* was expressed in the chicken forelimb ZPA (Figure 2-3C). However, unlike the situation in mice, *cTmem16a* was not detected in the chick hindlimb.

A previous cDNA microarray experiment identified the human ortholog of *TMEM16A* as a transcript expressed at elevated levels in gastrointestinal stromal tumors (GISTs) (Nielsen et al., 2002). Human *TMEM16A* is on chromosome 11q13, a region frequently amplified in esophageal cancer, bladder tumors, breast cancer (Katoh and Katoh, 2003), and oral squamous cell carcinomas (Huang et al., 2006). Murine *Tmem16a* was previously identified as the ortholog of human *TMEM16A*, but its *in vivo* expression had not previously been investigated (Katoh and Katoh, 2003).

Tcfap2b, Hlxb9, EST BI734840, and *Tmem16a* Are Expressed in *Shh* Null Limb Buds

After identifying genes with expression domains overlapping the ZPA, we used rtPCR to determine if their expression was *Shh*-dependent or *Shh*-independent. cDNA was synthesized from E11 wild type and *Shh* null limb buds and used as template to amplify fragments of *Tcfap2b*, *Hlxb9*, EST BI734840, and *Tmem16a*. All four transcripts were amplified from wild type and *Shh* null limb bud cDNA (Figure 2-3D). These data suggest that transcription of *Tcfap2b*, *Hlxb9*, EST BI734840, and *Tmem16a* is independent of *Shh* signaling.

Tmem16a Expression in the Limb is *Bmp*-Independent but Requires Ectodermal *Fgf* Expression

Members of the bone morphogenetic protein (BMP) family are essential for a number of developmental processes (Hogan, 1996). Recently, the removal of *Bmp2* and *Bmp4* from the limb mesenchyme was shown to result in soft tissue syndactyly and the loss of posterior digits in the forelimb (Bandyopadhyay et al., 2006). To determine if *Tmem16a* expression in the limb bud required BMPs, we analyzed expression of *Tmem16a* in limb buds in which both *Bmp2* and *Bmp4* had been removed from the mesenchyme. *Tmem16a* expression in *Bmp2c/c;Bmp4c/c;Prx1-cre* limbs was indistinguishable from the expression pattern observed in wild type littermates (Figure 2-4A,B).

Two fibroblast growth factors, *Fgf4* and *Fgf8*, are necessary for the initiation and outgrowth of the vertebrate limb (Boulet et al., 2004). Mice lacking both *Fgf4* and *Fgf8* in the AER were created using conditional alleles of *Fgf4* and *Fgf8* in conjunction with the ectoderm-specific cre allele *Msx2-cre* (Sun et al., 2002). Mice that lack both *Fgf4* and *Fgf8* in the ectoderm fail to develop hindlimbs. Interestingly, removal of these factors from the AER resulted in a complete loss of *Tmem16a* expression in the underlying hindlimb mesenchyme (Figure 2-4C,D). It has been shown that *Msx2-cre* expression in the forelimb occurs after expression of *Fgf8* has been initiated and that deletion of *Fgf8* with this cre allele leads to precocious expression of *Fgf4* (Sun et al., 2002). We observed a wild type expression pattern of *Tmem16a* in *Fgf4c/c;Fgf8c/c;Msx2-cre* forelimbs (data not shown).

Experimental Procedures

Fluorescence-Activated Cell Sorting of GFP-Positive Cells from the E10.5 Limb Bud

Mice heterozygous for the *Shhgfpcre* allele (Harfe et al., 2004) were crossed to wild type mice to generate heterozygous offspring. The morning a vaginal plug was found was considered E0.5. At E10.5, dams were sacrificed by cervical dislocation and the embryos harvested in ice-cold phosphate buffered saline (PBS). *Shhgfpcre* heterozygotes expressing green fluorescent protein (GFP) in the ZPA were identified using a fluorescent dissection microscope. Forelimbs and hindlimbs from heterozygous embryos were dissected from the body, pooled and placed in 0.05% trypsin at 37ºC for 5 minutes. The limbs were then triturated using a Pasteur pipette to obtain a single-cell suspension. The cells were centrifuged at 1,800 rpm for 2 minutes and resuspended in 0.5 uM EDTA, 0.05% BSA in PBS for sorting. GFP-positive and GFP-negative cells were collected using a FACS Vantage SE TurboSort (BD Biosciences, San Jose, CA). Approximately 1,000 GFP-positive (ZPA) cells were obtained from each limb bud which corresponded to ~3% of the cells sorted. A total of four cell sorts were performed to produce

four independent GFP-positive (ZPA cells) and GFP-negative (cells outside the ZPA) cell samples.

Microarray Target Preparation, GeneChip Hybridization, and Data Analysis

From each independent population of sorted cells, total RNA was isolated using the RNeasy Mini Kit (QIAGEN, Inc., Valencia, CA) according to the manufacturer's protocol. Sample integrity was assessed using an Agilent 2100 Bioanalyzer (Agilent Technologies, Inc., Santa Clara, CA) to compare the relative amounts of 18S and 28S rRNA. For each sample, 50 ng of total RNA was used as the starting material in the Affymetrix Two-Cycle cDNA Synthesis kit according to the Affymetrix Eukaryotic Target Preparation Manual (Affymetrix, Inc., Santa Clara CA). Following cleanup, biotin-labeled cRNA was synthesized using the Affymetrix GeneChip IVT Labeling Kit. For each sample, 15 ug of labeled cRNA was fragmented and hybridized to an Affymetrix Mouse Genome 430 2.0 GeneChip at 45ºC for 16 hours. The GeneChips were washed and stained with a GeneChip Fluidics Station 450 according to protocol EukGE Wsv4_450. A GeneChip Scanner 3000 was used to collect data into the GeneChip Operating Software (v1.3) using default parameters and global scaling as the normalization protocol. The trimmed mean target intensity was arbitrarily set at 500 for each GeneChip. This data has been made available from the Gene Expression Omnibus of the National Center for Biotechnology Information (http://www.ncbi.nlm.nih.gov/geo/ accession number GSE7598). To identify genes differentially expressed between the ZPA and the rest of the limb bud, we carried out a modified t-test on log transformed expression values using a random variance model as implemented in BRB ArrayTools developed by Richard Simon and Amy Peng Lam.

Whole Mount RNA *in situ* Hybridization and Generation of Mutant Embryos

Embryos were collected from timed matings for analysis by RNA *in situ* hybridization on E9.5, E10.5, E11.5, or E12.5. Embryos were fixed overnight at 4ºC in 4% paraformaldehyde in

PBS. RNA *in situ* hybridization was performed as described (Wilkinson, 1992). To analyze *cTmem16a* expression, HH19-24 chick embryos were harvested, fixed, and processed in an identical manner.

The expressed sequence tags (ESTs) used to generate antisense riboprobes for RNA *in situ* hybridizations can be found in Table 2-1. The plasmid used to generate the *Shh* riboprobe has been described previously (Echelard et al., 1993). The chicken EST chEST561F4 was used to generate a *cTmem16a* antisense riboprobe.

Generation of conditional alleles of *Bmp2* (Tsuji et al., 2006) and *Bmp4* (Liu et al., 2004) has been reported. To analyze *Tmem16a* expression in limbs lacking mesenchymal *Bmp2* and *Bmp4*, we crossed mice heterozygous for both conditional alleles that also carried a *Prx1-cre* transgene (Logan et al., 2002) to generate *Bmp2c/c;Bmp4c/c;Prx1-cre* offspring. Embryos were harvested at E10.5, genotyped as previously described for each allele, and fixed for RNA *in situ* hybridization. *Fgf4c/c;Fgf8c/c;Msx2-cre* embryos, which lack *Fgf4* and *Fgf8* expression in the AER, were a kind gift from Xin Sun (University of Wisconsin, Madison, WI).

rtPCR Analysis of Gene Expression

To confirm the expression of genes from Table 2-I we were unable to confirm by RNA *in situ* hybridization in the limb, wild type forelimbs were dissected into ice-cold TRIzol reagent (Invitrogen, Carlsbad, CA). RNA was isolated according to the manufacturer's protocol. cDNA was synthesized using AMV reverse transcriptase (Roche Applied Science, Indianapolis, IN), oligo dT oligonucleotides, and 5 ug of total RNA. Oligonucleotides used as PCR primers are listed in Table 2-3.

To verify gene expression in *Shh* null embryos, forelimb buds were dissected from wild type or *Shh* null E11.0 embryos and cDNA was synthesized as above. Oligonucleotides used as PCR primers are listed in Table 2-3.

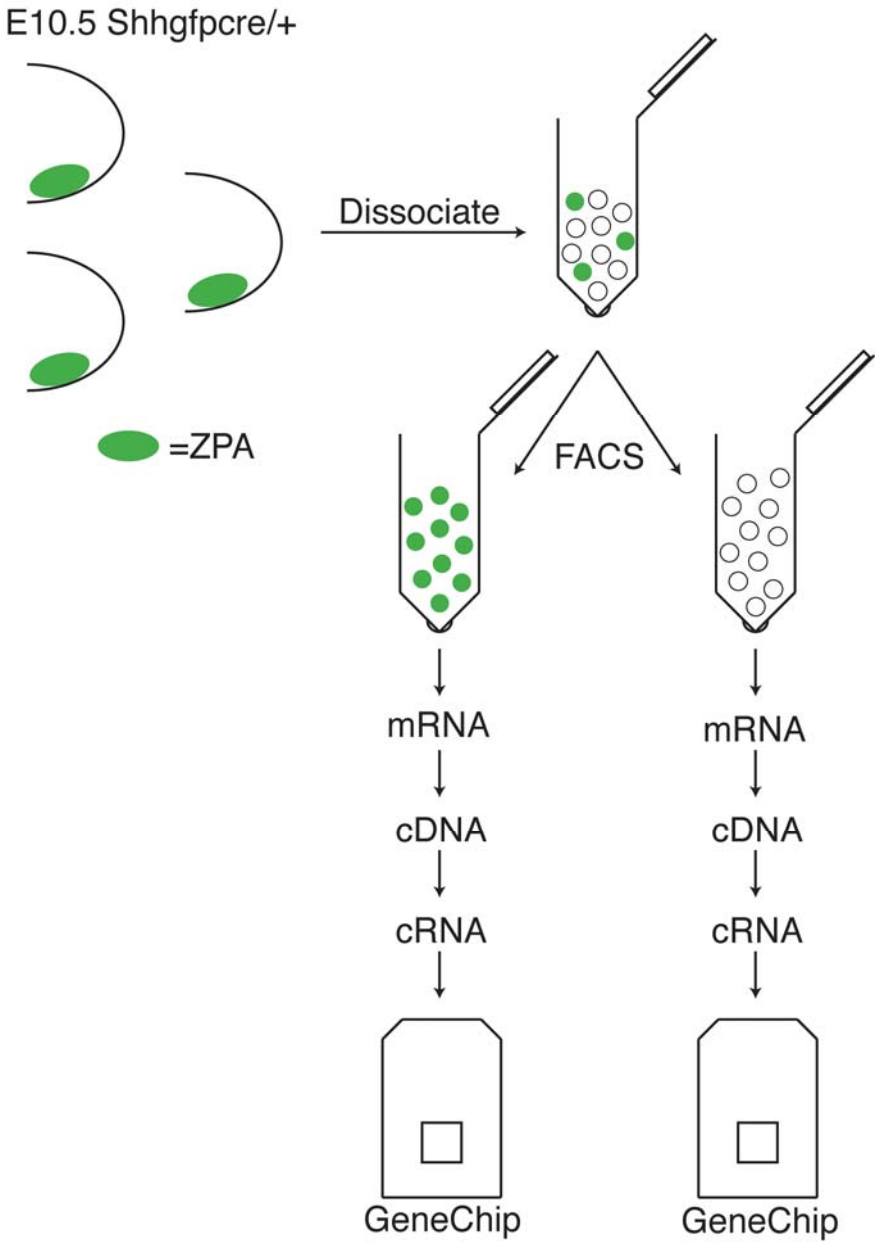

Figure 2-1. Analysis of gene expression in *Shh*-expressing cells of the ZPA and the rest of the E10.5 limb bud. Limbs were dissected from E10.5 *Shhgfpcre* heterozygous embryos and dissociated into single cells (see Experimental Procedures). GFP-positive (ZPA) and GFP-negative (rest of the limb) cell populations were purified by FACS. From these populations, labeled cRNA was synthesized and hybridized to Affymetrix GeneChips to compare whole-genome expression between cells of the ZPA and the cells of the rest of the limb. A total of eight GeneChips were used: four with purified ZPA cells and four with cells from the rest of the E10.5 limb bud.

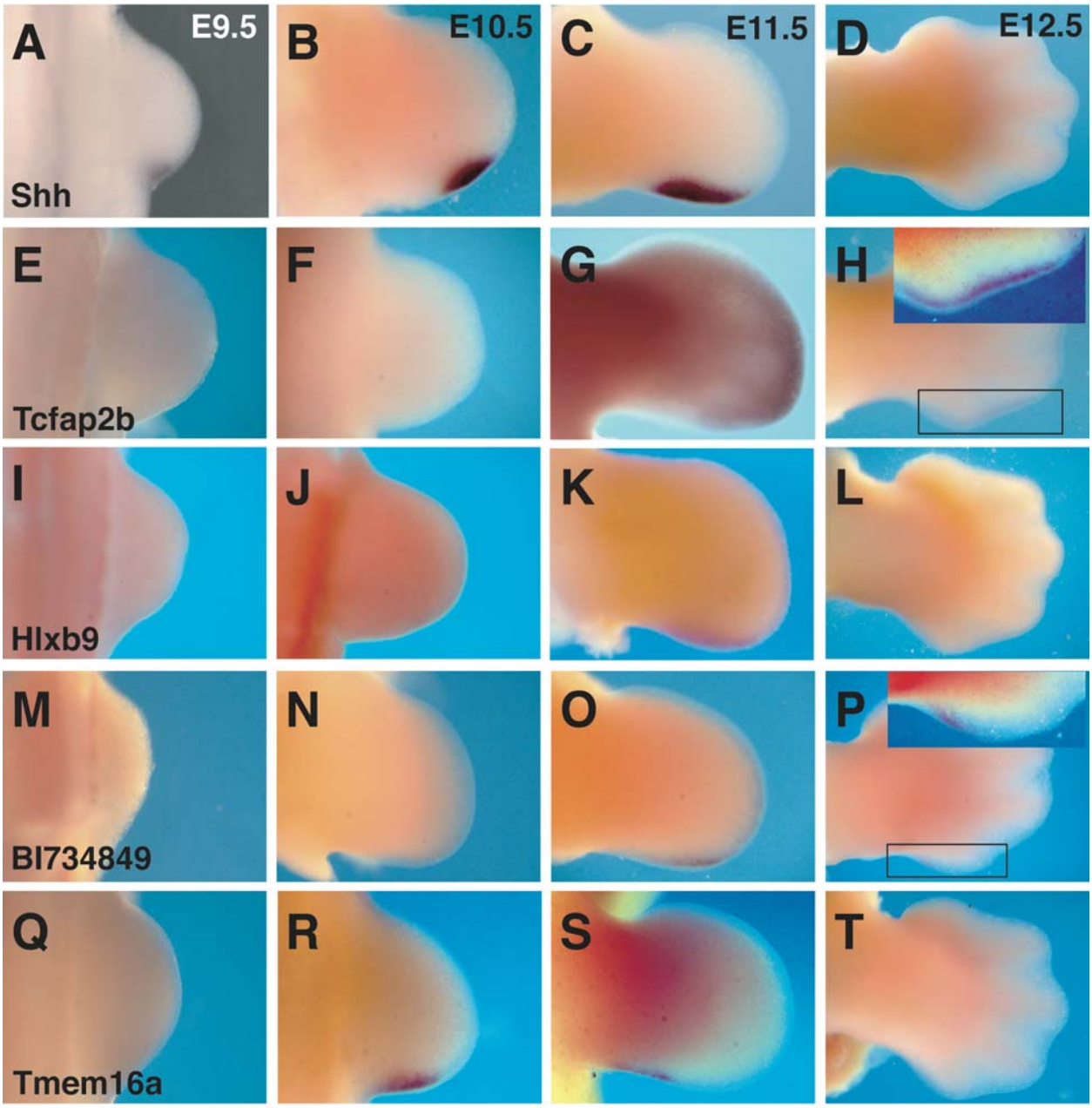

Figure 2-2. RNA *in situ* hybridization confirmed expression of four novel genes in the ZPA. Limbs from E9.5, E10.5, E11.5, and E12.5 wild type embryos were hybridized with probes corresponding to the list of genes whose expression is enriched in the ZPA from Table 2-1. *Shh* expression data is shown for comparison (A-D). *Tcfap2b* (G and H) and BI734849 (O and P) transcripts were detected on E11.5 and E12.5. *Hlxb9* expression was only observed on E11.5 (K). Expression of *Tmem16a* in the limb bud was observed in E10.5 and E11.5 limb buds (R and S).

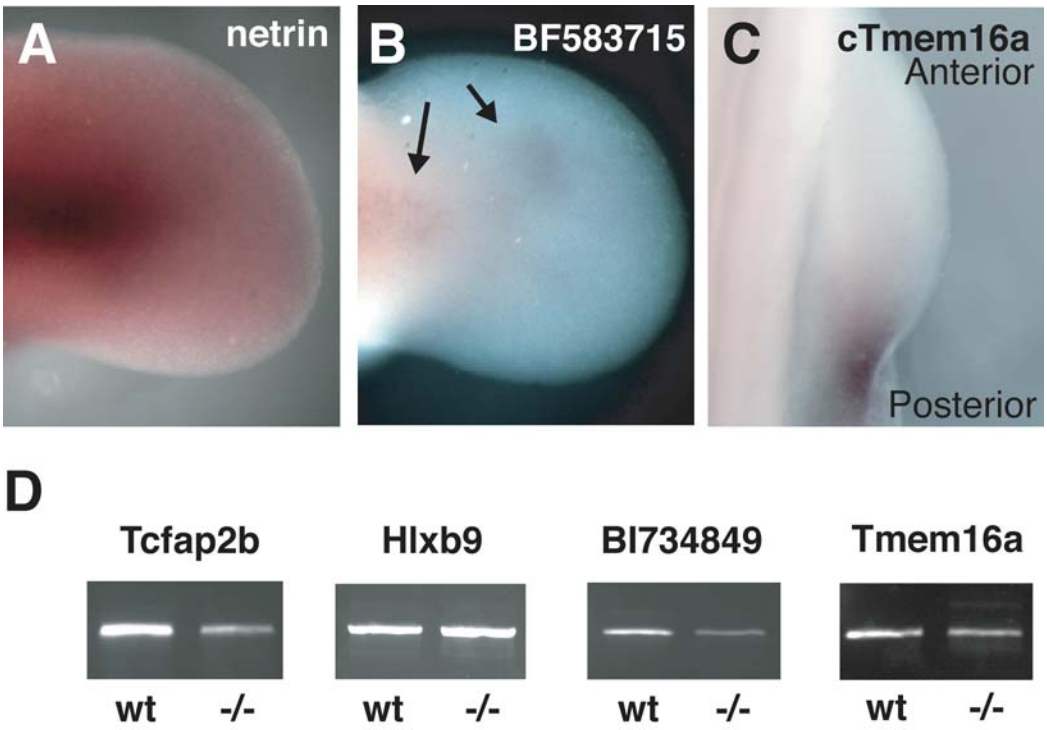

Figure 2-3. Further characterization of microarray data. RNA *in situ* hybridization detected transcripts of netrin (A) and the EST BF583715 (B) in the E11.5 limb bud. Consistent with the microarray data, these transcripts were detected in the limb bud but not in the ZPA. (C) *cTmem16a* expression was observed in the ZPA of chicken forelimbs (HH19 shown), but not in the hindlimbs at any stage examined (HH19-24). (D) rtPCR demonstrated that expression of *Tcfap2b*, *Hlxb9*, EST BI734849, and *Tmem16a* occurs in both wild type and *Shh* null forelimbs from E11.0 embryos.

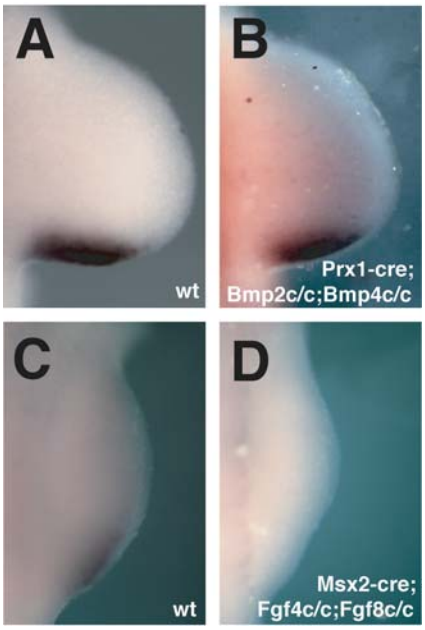

Figure 2-4. *Tmem16a* expression in the limb is *Bmp*-independent but requires ectodermal *Fgf* expression. RNA *in situ* hybridization showed that the pattern of *Tmem16a* expression was not changed in E10.5 *Bmp2c/c;Bmp4c/c;Prx1-cre* (B) forelimbs when compared to wild type littermates (A). In contrast, *Tmem16a* expression was lost from the hindlimb AER in *Fgf4c/c;Fgf8c/c;Msx2-cre* embryos (D).

Table 2-1. Partial list of genes identified as enriched in the ZPA or outside of the ZPA in the E10.5 limb bud.

Affymetrix Probe Set ID	Annotation	Geometric mean of intensities (GFP-negative/GFP-positive)	p-value	Probe	Confirmed by *in situ*	Confirmed by rtPCR
Genes enriched in ZPA						
1419473_a_at	*Cck*	0.044	5.09E-05	BU560753	No	
1459713_s_at	*Tmem16a*	0.024	2.52E-03	BC006062	Yes	
1436981_a_at	*Ywhaz*	0.114	5.74E-03	BQ044210	No	Yes
1420784_at	*Scn11a*	0.11	7.15E-03	BG694370	No	
1437418_at	*Ncrms*	0.157	5.42E-02	BI734849, AI853140	Yes	
1435670_at	*Tcfap2b*	0.26	8.77E-02	AI585585	Yes	
1436450_at	D11Bwg0517e	0.313	1.12E-01	BU563678	No	
1460299_at	*Hlxb9*	0.223	1.27E-01	BE648171	Yes	
1431328_at	*Ppp1cb*	0.509	1.67E-01	CB723562	No	Yes
Genes enriched outside the ZPA						
1424214_at	9130213B05Rik	14.705	3.01E-03	BF583715	Yes	

Analysis of the array data resulted in the identification of a large number of genes differentially expressed between the ZPA and the rest of the limb bud. From this list, we chose 9 genes that were enriched in the ZPA and 1 gene that was enriched in the rest of the limb to confirm by RNA *in situ* hybridization. These genes were ranked by the probability that each is differentially expressed between the two cell populations (p-value). For those genes enriched in the ZPA, ratios of geometric means closest to zero suggest highest expression levels in the ZPA compared to the rest of the limb. The ESTs used to generate *in situ* riboprobes are shown.

Table 2-2. Genes previously described in the limb identified by the ZPA screen.

Affymetrix Probe Set ID	Annotation	Geometric mean of intensities (GFP-negative/GFP-positive)	p-value	Probe
Genes enriched in ZPA				
1422912_at	*Bmp4*	0.125	2.22E-04	
1436869_at	*Shh*	0.047	4.46E-04	
1422545_at	*Tbx2*	0.25	8.14E-04	
1450584_at	*Hoxd11*	0.278	3.65E-03	
1446812_at	*Hand2*	0.388	1.78E-02	
1439663_at	*Ptch1*	0.187	2.44E-02	
1422239_at	*Hoxd13*	0.176	6.24E-02	
1423635_at	*Bmp2*	0.214	1.27E-01	
1449058_at	*Gli1*	0.636	2.56E-01	
Genes enriched outside the ZPA				
1454974_at	*Ntn1*	66.635	3.80E-06	BE196965
1424950_at	*Sox9*	18.883	6.26E-03	
1425357_a_at	*Grem1*	2.781	3.34E-02	

Table 2-3. Oligonucleotide primers used for rtPCR.

Tcfap2b		
	F	5'-CACTAACAGGCACACGTCTG-3'
	R	5'-CGTCTCAGTCAACCAGCTCTC-3'
Hlxb9		
	F	5'-ATTTGGTTCCAGAACCGCCGAATG-3'
	R	5'-TGGTTGTCTCCAAAGGAGGGTTCA-3'
BI734849		
	F	5'-CCAGAATGACTGTGTAGCTC-3'
	R	5'GAAGGATCTGCCAAGCTCAC-3'
Tmem16a		
	F	5' CAAGTTTGTGAACTCTTA
	R	5' TCGGGCGTGAGGCCGGCGAAAG
Ppp1cb		
	F	5' GAACGTGGACAGCCTCATCAC
	R	5' GATGCTAGCACACTCATG
Ywhaz		
	F	5' GACGCCGAGCTCGCGACTGG
	R	5' CATAACTGGATATTCTGTGTCC

CHAPTER 3
DEFECTIVE TRACHEAL CARTILAGE RING FORMATION CAUSED BY DELETION OF THE TRANSMEMBRANE PROTEIN TMEM16A

Pathological collapsibility of the upper airways, known as tracheomalacia in humans, can occur either independently or in combination with other anomalies. Depending on its etiology and severity, the symptoms of tracheomalacia range from respiratory stridor to fatal airway obstruction. Since the clinical presentations of tracheomalacia are so diverse, the condition is often misdiagnosed or not diagnosed at all and its true incidence is not known. We determined that *Tmem16a*, a member of an uncharacterized evolutionarily conserved family of predicted transmembrane proteins, is expressed in the epithelium of the developing trachea. To investigate the role of *Tmem16a* in tracheal development, we generated a null allele of this gene in mice. All mice homozygous for this null allele exhibited severe tracheomalacia with gaps in the tracheal cartilage rings along the entire length of the trachea. We show that the embryonic tracheal epithelium was improperly stratified in *Tmem16a* mutants and this caused an expansion of the tracheal lumen. The expanded epithelial tube displaced chondrogenic condensations in the surrounding mesenchyme and caused the malformation of the tracheal cartilage rings. These data identify *Tmem16a* as a novel regulator of epithelial organization in murine tracheal development. Furthermore, this mutant, the first knockout of a vertebrate TMEM16 family member, provides a mouse model of tracheomalacia.

Introduction

The murine respiratory system is first recognizable as two primary lung buds emerge from the ventral foregut endoderm on embryonic day (E) 9.5 (reviewed in (Cardoso and Lu, 2006)). These buds elongate and branch in a reiterative process, known as branching morphogenesis, to generate the distal respiratory tree. The foregut endoderm rostral to the site of the primary lung buds gives rise to two epithelial tubes: the esophagus and trachea. The mechanisms governing

the separation of these two tubes are not entirely clear, but errors in this process carry significant clinical implications in the forms of tracheoesophageal fistula and esophageal atresia (Que et al., 2006).

C-shaped rings of hyaline cartilage encircle the ventrolateral surfaces of the mature trachea and prevent its collapse during respiration. In humans, structural weakness of the trachea, known as tracheomalacia, results in collapse of the airway during respiration (for reviews see (Carden et al., 2005; McNamara and Crabbe, 2004)). Depending on the degree of tracheal collapse, symptoms range from respiratory stridor to fatal airway obstruction. The true incidence of tracheomalacia is not known because many of its symptoms overlap with those of other pulmonary disorders and it is often misdiagnosed; however, estimates range from 1 in 2,600 to 1 in 1,445 births (Boogaard et al., 2005; Carden et al., 2005). In some instances, tracheomalacia arises through developmental malformation of the trachea itself; this congenital form is known as primary trachemalacia (reviewed in (Carden et al., 2005)). Examples of primary tracheomalacia include defects in cartilage matrix production or the shortened cartilage elements observed in patients with tracheoesophageal fistula. In other cases, classified as secondary tracheomalacia, the cause of tracheal collapse is extrinsic to the trachea. Examples of secondary tracheomalacia include trauma and external pressure on the trachea from adjacent organs.

In mice, the tracheal cartilage rings develop in the splanchnic mesenchyme surrounding the trachea between embryonic day (E) 13.5 and E15.5 (Miller et al., 2004). Very little is currently known about the embryology of the tracheal cartilage rings, but reverse genetic experiments in mice have identified several genes that affect their development. These include *Shh* (Miller et al., 2004), *Hoxa-5* (Aubin et al., 1997), *Traf4* (Regnier et al., 2002), *FoxF1* (Mahlapuu et al., 2001), *Raldh2* (Vermot et al., 2003) and various retinoic acid receptors (Mendelsohn et al.,

1994). Unfortunately, the characterizations of these mutants have focused on other defects and the mechanisms underlying their tracheal cartilage malformations have not been investigated in detail.

Tmem16a is a member of the TMEM16 family of proteins with orthologs in organisms ranging from *Saccharomyces cerevisiae* to humans (Entian et al., 1999) (Katoh and Katoh, 2003). Human *TMEM16A* (other published names for this protein include *DOG1, TAOS2* and *FLJ10621*) is amplified in a number of cancers including oral squamous cell carcinoma and gastrointestinal stromal tumors (Huang et al., 2006) (West et al., 2004). Despite this evolutionary conservation and potential clinical significance, the functions of the vertebrate TMEM16 proteins are unknown.

We report that murine *Tmem16a* is expressed in the epithelium of the developing trachea and that mice homozygous for a null allele of *Tmem16a* failed to thrive during postnatal life. These mice exhibited severe primary tracheomalacia with ventral gaps in the tracheal rings along the entire rostrocaudal axis of the trachea. The cells of the tracheal epithelium in *Tmem16a* mutants were improperly organized during embryogenesis and the trachea expanded into the surrounding mesenchyme. This abnormal expansion of the trachea partitioned the normal chondrogenic C-shaped rings into multiple chondrogenic condensations in *Tmem16a* mutants. This phenotype resulted in symptoms that mimic those in humans with tracheomalacia.

Results

Tmem16a Is Expressed in the Tracheal Epithelium

We performed whole mount and section RNA *in situ* hybridizations with an antisense riboprobe to detect *Tmem16a* transcripts during murine tracheal development. At E10.5 we observed *Tmem16a* expression throughout the epithelia of the foregut and primary lung buds (Figure 3-1A). *Tmem16a* expression continued in the proximal airway epithelium (trachea and

conducting airways of the lung) at E11.5 and E12.5, but was absent from the distal tips of peripheral lung epithelium at these stages (Figure 3-1B,C,D). At E14.5 and E16.5 *Tmem16a* expression was detected in cells of the tracheal epithelium (Figure 3-1E,F). In addition to epithelial expression, intense signal was observed in the mesenchyme dorsal to the trachea (Figure 3-1D,E,F). This dorsal mesenchyme does not form cartilage but instead forms the trachealis muscle which bridges the gaps in the cartilage rings. *Tmem16a* expression was not detected in the chondrogenic mesenchyme of the ventrolateral trachea at any stage examined (E10.5-E18.5).

Tmem16a Null Mice Fail to Thrive During Postnatal Life

To investigate the functions of *Tmem16a* in vertebrate development, we generated a null allele of this gene by homologous recombination in murine embryonic stem (ES) cells (Figure 3-2A). Our targeting strategy removed 53 amino acids of the second (of eight) predicted transmembrane domains and the extracellular loop between the first and second transmembrane domains. This strategy also induced a frameshift mutation 3' of the deletion, which resulted in the creation of a termination codon 40 amino acids downstream of the deletion. One correctly targeted ES cell clone was identified by Southern blot and these cells were used to generate chimeric animals by blastocyst injection. Germline transmission of this allele, $Tmem16a^{tm1Bdh}$, was confirmed by polymerase chain reaction (PCR). Mice heterozygous for $Tmem16a^{tm1Bdh}$ had no apparent phenotype and were mated to generate homozygous offspring.

Greater than 90% of $Tmem16a^{tm1Bdh/tm1Bdh}$ pups (hereafter referred to as *Tmem16a* mutants) died within the first nine days of postnatal life and no *Tmem16a* mutants survived longer than 30 days postpartum (Figure 3-2B and data not shown). *Tmem16a* mutants were born with the expected Mendelian frequency (19/81 or 27%) and newborn mutants had a body weight similar to that of wild type and heterozygous littermates (Figure 3-2C). However, *Tmem16a* null

animals did not gain weight at the same rate as their littermates (Figure 3-2C). Three days after parturition, *Tmem16a* mutants weighed only ~65% as much as their littermates. *Tmem16a* nulls that survived 21 days postpartum weighed less than half as much as wild type littermates. Milk was observed in the stomachs of *Tmem16a* null pups suggesting that these pups were able to locate nipples and initiate suckling behavior.

A portion of *Tmem16a* null pups developed grossly distended bellies within the first postnatal week. Varying amounts of air were encountered in the esophagi, stomachs, and intestines of all *Tmem16a* null pups upon sacrifice and subsequent dissection (data not shown). This aerophagia was frequently associated with a cyanotic appearance prior to sacrifice and suggested a defect in the development of the upper respiratory and/or digestive tracts in *Tmem16a* mutants. Neither gross nor histological examination of craniofacial development revealed any obvious patterning defects of the palate, tongue, larynx, or crania of *Tmem16a* null pups (data not shown).

Tmem16a Mutants Exhibit Defects in Tracheal Cartilage Ring Formation

Because *Tmem16a* was expressed in the developing trachea and the mutant phenotype was consistent with an upper airway anomaly, tracheae were dissected from *Tmem16a* mutants and littermates and stained with alcian blue to examine cartilage elements. Ventral gaps were observed along the entire rostocaudal axis of mutant tracheae and the cartilage plates on the bronchi were also abnormally patterned (Figure 3-2D and data not shown). This phenotype was 100% penetrant in *Tmem16a* mutants; however, the pattern of rudimentary cartilage elements was variable. Transverse sections of *Tmem16a* mutant tracheae stained with alcian blue and eosin demonstrated multiple lateral cartilage condensations with intervening epithelial evaginations (compare Figure 3-2E and F). Development of the thyroid and cricoid cartilages was not disrupted (Figure 3-2D and data not shown).

Chondrogenic Cells Are Present in the Ventral Mesenchyme of *Tmem16a* Mutants

Tracheal cartilage rings develop in the splanchnic mesenchyme surrounding the trachea between E13.5 and E15.5 (Miller et al., 2004). Expression of *Sox9*, a high mobility group transcription factor, has been reported in cells fated to form cartilage in the peritracheal mesenchyme beginning at E9.0 (Elluru and Whitsett, 2004). Immunohistochemistry and RNA *in situ* hybridization revealed that *Sox9* positive cells were present in the ventrolateral tracheal mesenchyme of both wild type and *Tmem16a* mutant embryos at E12.5 and E13.5 (Figure 3-3A,B,D,E and data not shown). This suggested that, similar to the situation in wild type, the ventral mesenchymal cells in *Tmem16a* mutants were specified to undergo chondrogenesis. However, at E14.5 the tracheal epithelium was noticeably thinner and had evaginated into the ventrolateral mesenchyme of *Tmem16a* mutants. This evagination aberrantly partitioned the *Sox9* positive cells into separate populations (compare Figure 3-3C and F).

The evagination of the tracheal epithelium and disruption of the mesenchymal chondrogenic condensations was not due to ectopic cell death or cell proliferation. TdT-mediated dUTP nick end labeling (TUNEL) did not reveal any apoptotic nuclei in mutant tracheae at any stage examined (data not shown). In addition, 5'-bromo-2'-deoxyuridine (BrdU) incorporation did not reveal a change in the proliferative indices of mutant tracheal mesenchyme (or epithelium) at E13.5 or E14.5 (data not shown).

Sox9 has been shown to directly activate transcription of genes encoding cartilage components such as *Col2a1* (Lefebvre et al., 1997) and aggrecan (Sekiya et al., 2000). In E15.5 wild type embryos, immunohistochemistry revealed a single population of type II collagen positive chondrocytes in a C-shaped ventrolateral ring (Figure 3-3G). In stark contrast, two or more type II collagen positive condensations were observed at this stage in mutants with intervening epithelial evaginations (Figure 3-3H). These data together suggested that

prechondrocytes were present in the mutant ventral tracheal mesenchyme but ultimately were redirected by an abnormal epithelium to contribute to disconnected lateral chondrogenic condensations.

Increased Tracheal Circumference in *Tmem16a* Null Mice

Epithelial evaginations occurred along the entire rostrocaudal axis of *Tmem16a* mutant tracheae (Figures 3-2D,F and 3-3) and we reasoned this could result from an increase in the circumference of the epithelial tube. In addition, the lumens of mutant tracheae appeared dilated in comparison to those of wild type tracheae (see Figures 3-3 and 3-4). To quantify this defect, we photographed transverse histological sections of tracheae from *Tmem16a* mutants and littermates at E13.5 and E14.5 at the same relative rostrocaudal location. For each image, the luminal circumference of the trachea was measured by outlining the apical surface of the tracheal epithelium using image analysis software (see Experimental Procedures). At E13.5, the luminal circumference was nearly 40% greater in mutants (n=2) than in wild type and heterozygous controls (n=2) (Figure 3-3I). This defect was even more severe in E14.5 embryos where the epithelial circumference of *Tmem16a* mutants (n=2) was nearly 75% larger than heterozygous littermates (n=2) (Figure 3-3I).

Ciliated Cells Are Absent from Evaginated Regions of the Tracheal Epithelium

The disorganization of *Tmem16a* mutant tracheal epithelium might have been attributable to abnormal differentiation of epithelial cell types. Ciliated columnar cells and non-ciliated secretory Clara cells are abundant in the mature tracheal epithelium of the mouse (Rawlins and Hogan, 2006). Although a population of *p63*-expressing cells is found in the wild type embryonic tracheal epithelium, mature basal cells are not established until late gestation (Daniely et al., 2004). To assess differentiation, we immunolocalized markers of epithelial cell types in mutant and wild type newborn tracheae.

Acetylated a-tubulin is localized to the cilia on the apical surfaces of epithelial cells in the trachea (Gomperts et al., 2004). Immunofluorescence on newborn wild type trachea sections revealed an even distribution of ciliated cells around the tracheal epithelium (Figure 3-4A). In *Tmem16a* mutant trachea, we observed ciliated cells in the tracheal epithelium with a relatively normal distribution (Figure 3-4B); the one exception was the evaginated epithelium that persisted until birth. These regions of the mutant tracheae were conspicuously devoid of ciliated cells (arrow in Figure 3-4B). Since ciliated cells were present throughout most of the mutant trachea, we propose that this is the result of the juxtaposition of two apical surfaces and not a defect in specification of the ciliated lineage. Apical localization of ezrin, a member of the ERM (ezrin, radixin, moesin) protein family, precedes the formation of cilia in tracheal epithelium in air-liquid interface conditions (Huang et al., 2003). We observed normal apical distribution of ezrin in ciliated cells of *Tmem16a* mutants (data not shown).

Clara cells of the murine tracheal epithelium can be identified by the presence of the secretoglobin *Scgb1a1* (Perl et al., 2005). We detected Clara cells throughout the tracheal epithelium of newborn wild type and *Tmem16a* mutant pups (Figure 3-4A,B). In particular, we detected *Scgb1a1*-expressing cells in regions of trachea that had undergone abnormal epithelial evagination.

In the mature pseudostratified epithelium of the mouse trachea, a population of basal cells can be identified by their expression of the transcription factor *p63* (Daniely et al., 2004). As a multipotent progenitor cell type of the proximal airways, basal cells are capable of restoring tracheal epithelial cell diversity following injury (Hong et al., 2004). In newborn mice, we observed a normal distribution of *p63*+ basal cells in *Tmem16a* mutant tracheal epithelium (Figure 3-4C,D).

Embryonic Tracheal Epithelium Stratification Is Lost in *Tmem16a* Mutants

Since we did not observe a change in proliferation, apoptosis or differentiation in *Tmem16a* mutant tracheal epithelium, we reasoned that the luminal expansion could result from an abnormal arrangement of epithelial cells. The mid-gestational tracheal epithelium of the mouse is reported to comprise 2 to 3 cell layers (Daniely et al., 2004). To assess tracheal epithelium organization in *Tmem16a* mutants, we performed immunofluorescence on transverse sections of *Tmem16a* mutant and wild type trachea with a *Cdh1* antibody to identify basolateral epithelial cell plasma membranes. Sections were counterstained with 4',6-Diamidino-2'-phenylindole (DAPI) to reveal nuclei. In contrast to the stratified epithelium of the E14.5 wild type trachea, a majority of the nuclei in the mutant tracheae were located adjacent to the basement membrane (Figure 3-4E-H). As a result of this lateral arrangement of cells, the epithelium was observably thinner. These data support a mechanism in which the embryonic epithelium of *Tmem16a* mutants fails to achieve proper stratification and, as a result, an increase in epithelial circumference and expansion of the tracheal lumen occurs.

Discussion

Abnormal Morphogenesis of the Tracheal Epithelium in *Tmem16a* Mutants

We report that mice lacking the transmembrane protein TMEM16A demonstrate defects in organization of the tracheal epithelium during embryogenesis. The cells of the epithelium fail to stratify and most nuclei are located in close proximity to the basement membrane. The defective stratification is not the result of a global loss in apicobasal polarity or improper localization of proteins to the apical surface; in ciliated cells of *Tmem16a* mutant tracheae, both the cilia and the cytoskeletal linker protein ezrin were properly localized to the apical surface. Furthermore, we demonstrated normal differentiation of Clara cells, ciliated cells, and basal cells in mutant tracheae.

Previous experiments have shown that oriented and asymmetric cell divisions are necessary for stratification of the skin (Lechler and Fuchs, 2005). One possibility is that similar asymmetric cell divisions are also necessary for tracheal epithelial stratification and require TMEM16A. In support of this hypothesis, IST2, the only TMEM16 ortholog identified in the yeast *Saccharomyces cerevisiae*, has been shown to sort asymmetrically during budding (Takizawa et al., 2000). This protein, however, is distantly related to TMEM16A and does not necessarily share the same function or distribution.

One vertebrate paralog of TMEM16A, TMEM16E, has been localized primarily to intracellular membranes in cultures of myotubes (Mizuta et al., 2007). For the paralog TMEM16G (also known as NGEP), one splice isoform has been reported intracellularly while a second isoform has been identified on the plasma membrane (Bera et al., 2004). These data suggest that TMEM16A may function either at an intracellular membrane and/or at the plasma membrane. If TMEM16A does function at the plasma membrane, it is possible that this protein plays a role in mediating cell-cell contacts or intercellular communication. Interestingly, the paralog TMEM16G has been shown to promote adhesion between LNCaP cells in culture where it is localized to the apical and lateral surfaces (Das et al., 2007). A loss of adhesion between *Tmem16a* mutant cells could explain the lateral arrangement of cells and lack of stratification of *Tmem16a* mutant trachea epithelium.

A Novel Etiology for Tracheomalacia in a Murine Model

The formation of tracheal cartilage rings normally occurs in the ventrolateral mesenchyme around the tracheal epithelium during mid-embryogenesis. One consequence of the improper organization of *Tmem16a* mutant tracheal epithelium was an expansion of the epithelial circumference. This, in turn, caused evaginations of the tracheal epithelium into the surrounding mesenchyme that disrupted the chondrogenic condensations of the tracheal cartilage rings.

Instead of the C-shaped rings required to prevent the trachea from collapsing during normal respiration, multiple cartilaginous rudiments formed along the entire length of the trachea. This abnormal arrangement of tracheal cartilage contributed to the aerophagia, cyanosis, and failure to thrive of postnatal *Tmem16a* mutants. In humans, tracheomalacia is exacerbated by esophageal expansion during feeding and can lead to a failure to thrive similar to what we observed in *Tmem16a* mutant mice (Ahel et al., 2003).

In mice, previous reports have concluded that deletion of factors from the tracheal epithelium can result in malformation of the tracheal cartilage rings by disrupting paracrine signaling to the surrounding mesenchyme (Miller et al., 2004; Regnier et al., 2002). We propose that in addition to this established role of paracrine signaling between the epithelium and mesenchyme, the physical interaction of these two tissues also drastically affects tracheal development. We propose that tracheomalacia in *Tmem16a* mutants is the result of mechanical force exerted by an abnormal epithelial tube during development of the tracheal cartilage rings in the surrounding mesenchyme.

In humans, the diagnosis of tracheomalacia is complicated because its symptoms overlap with those of other pulmonary disorders and there is no single etiology for this condition. In many cases of tracheomalacia, the condition is self-limiting and conservative treatment is favored (Carden et al., 2005; Greenholz et al., 1986). In more severe cases, treatment including ventilation and surgery are required. In addition to identifying a novel etiology for tracheomalacia, the *Tmem16a* mutant mice provide a murine model of severe primary tracheomalacia that could be used to aid in the diagnosis and treatment of this condition.

Currently, very little is known about the embryology and molecular biology of normal tracheal development. We demonstrate that there is a requirement for stratification of the mid-

gestational tracheal epithelium in normal development and identify *Tmem16a* as a novel mediator of this process. Furthermore, we show that TMEM16A is required for normal development of the tracheal cartilage rings and that loss of this protein results in tracheomalacia.

Experimental Procedures

Generation of a Null Allele of *Tmem16a*

Arms of homology flanking exon 12 of *Tmem16a* were PCR amplified from CJ.7 ES cell genomic DNA and cloned into an ES cell targeting vector containing a floxed PGK-neo cassette. The linearized targeting construct was electroporated into 129S1/SvImj derived CJ.7 ES cells (Swiatek and Gridley, 1993) and targeted clones were enriched for by selection with Geneticin (Invitrogen, Carlsbad, CA) and FIAU (Moravek Biochemicals, Brea, CA). Southern blotting confirmed the correct targeting of one ES cell line that was used to generate chimeras by blastocyst injections. Germline transmission of the correctly targeted allele was confirmed by PCR. All experiments were approved by and performed according to the regulations of the Institutional Animal Care and Use Committee of the University of Florida.

Dams or pups were sacrificed by cervical location or carbon dioxide asphyxiation, respectively, and embryos or tracheae were isolated in PBS prior to fixation overnight at 4ºC in 4% paraformaldehyde. Samples were dehydrated, infiltrated with HistoWax (Leica Microsystems, Bannockburn, IL), and embedded in paraffin. 7µm sections were cut on a rotary microtome.

Alcian Blue Staining of Cartilage

Whole tracheae or dewaxed and rehydrated 7µm paraffin sections were stained in 0.03% alcian blue (Fisher Scientific, Pittsburgh, PA) in 25% glacial acetic acid in ethanol. Whole mount samples were cleared by immersion in KOH and glycerol. Sections were counterstained in eosin, dehydrated, and mounted.

RNA *in situ* Hybridization

RNA *in situ* hybridizations were performed on whole lungs or 14µm cryosections according to an adapted standard protocol (Nieto et al., 1996). The plasmid used to generate antisense probe for *Tmem16a* has been described previously (Rock et al., 2007).

Immunohistochemistry and Immunofluorescence

Sections were dewaxed and rehydrated. Antigen retrieval was performed by microwaving slides for 20 minutes in 10mM citric acid (pH6.0) with 0.05% Tween-20 (Fisher Scientific, Pittsburgh, PA). Primary antibodies were from Santa Cruz Biotechnologies (Santa Cruz, CA) and were used at the following concentrations: Rabbit anti-Sox9 at 1:200 (sc-20095), goat anti-Collagen Type II at 1:200 (sc-7764), goat anti-CC10 at 1:100 (sc-9772) (CC10 is also known as Scgb1a1), mouse anti-p63 at 1:200 (sc-8431). Other primary antibodies used included the following: rat anti-Cdh1 at 1:200 (U3254, Sigma, St. Louis, MO) and mouse anti-acetlyated a-tubulin at 1:100 (Ab24610, Abcam, Cambridge, MA). p63 was visualized using the MOM kit and Sox9 and Collagen Type II were visualized using VectaStain ABC kits (Vector Laboratories, Burlingame, CA) and metal-enhanced DAB (Pierce Biotechnology, Rockford, IL). Sections were counterstained with eosin or Richardson's Azure II. Secondary antibodies for immunofluorescence were: Cy2-conjugated donkey anti goat, Cy3-conjugated donkey anti-rat, and Cy3-conjugated donkey anti-mouse (Jackson ImmunoResearch, West Grove, PA). 4',6-Diamidino-2'-phenylindole (DAPI, Pierce Biotechnology, Rockford, IL) was used as counterstain.

Image Acquisition and Measurement of Luminal Circumference

Images were acquired using a Lecia DFC300 FX camera or Leica TCS SP2 confocal system (Leica Microsystems, Bannockburn, IL). For luminal measurement, images of histological sections of wild type and *Tmem16a* mutant tracheae were visualized in ImageJ

(National Institutes of Health). The apical epithelial surface for each image was traced and converted from pixels to μm by measuring a micrometer in an identical manner. Single litters were analyzed to minimize variation due to staging and processing. Data shown is average +/- s.e.m.

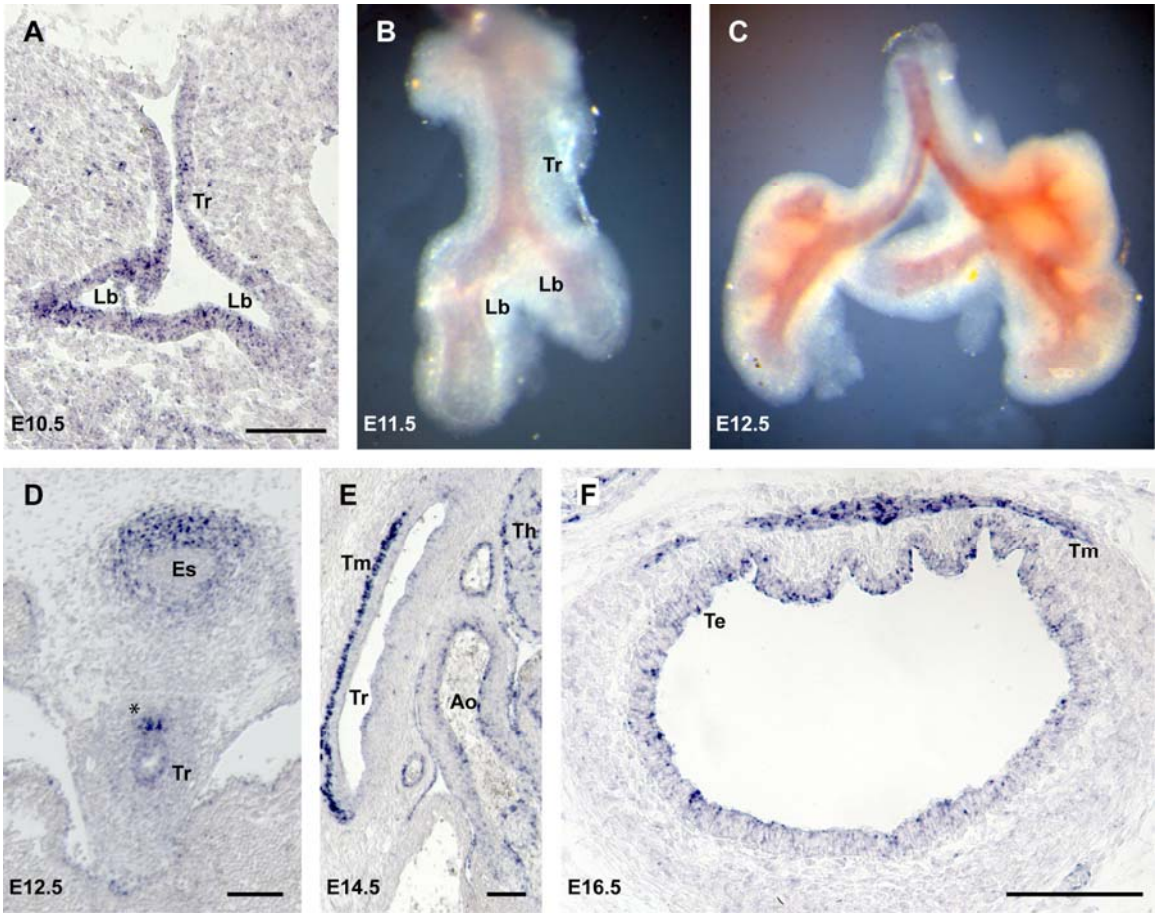

Figure 3-1. *Tmem16a* is expressed in the developing tracheal epithelium. A. RNA *in situ* hybridization on wild type E10.5 cryosection demonstrated *Tmem16a* expression throughout the foregut endoderm and primary lung buds. Whole mount RNA *in situ* hybridization showed *Tmem16a* expression persisted in the epithelium of the trachea and conducting airways of the lung at E11.5 (B) and E12.5 (C). D. Section RNA *in situ* hybridization showed *Tmem16a* expression in the tracheal epithelium and the mesenchyme dorsal to the trachea (asterisk in D) at E12.5. Expression of *Tmem16a* in the tracheal epithelium continued at E14.5 (E) and E16.5 (F). Robust *Tmem16a* expression was also observed in the developing trachealis muscle at these stages (E,F). *Tmem16a* expression was also observed in the esophagus, aorta and thymus (D, E and data not shown). Abbreviations: Tr, trachea; Lb, lung bud; Es, esophagus; Ao, aorta; Th, thymus; Te, tracheal epithelium; Tm, trachealis muscle. Scale bars=100μm.

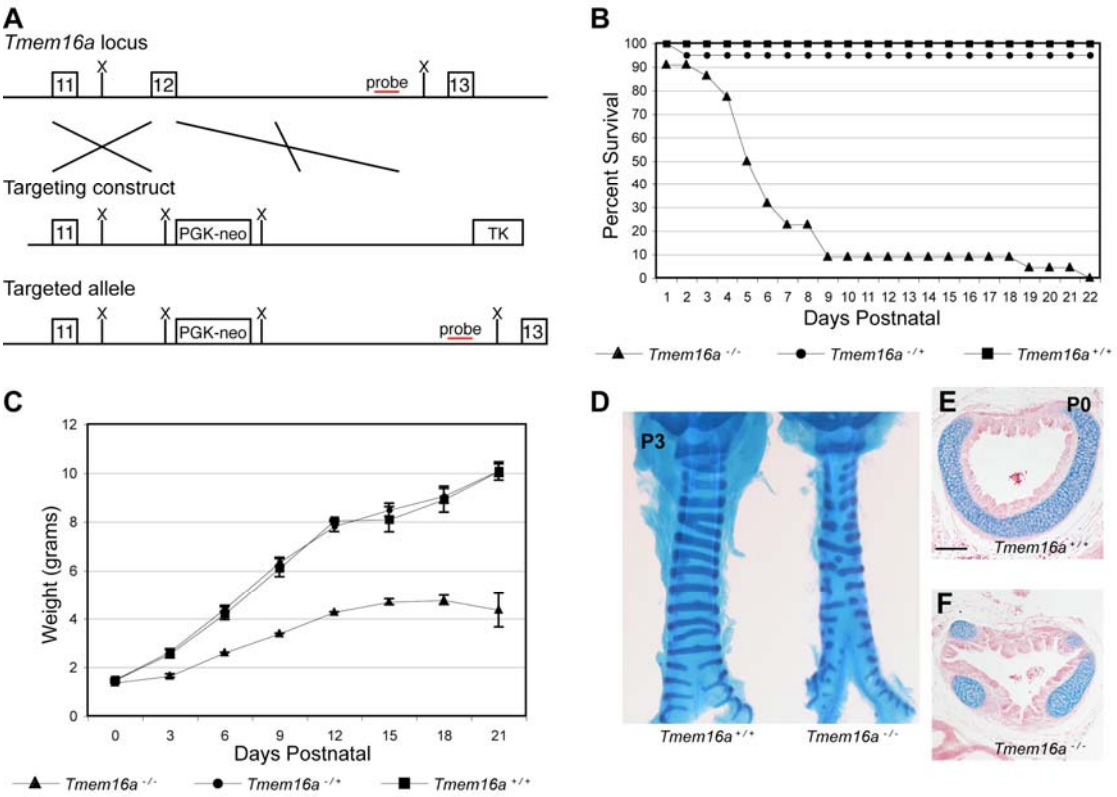

Figure 3-2. *Tmem16a* null mice die within the first month of life and do not complete normal tracheal development. A. Exon 12 of *Tmem16a* was replaced with a PGK-neo cassette by homologous recombination in embryonic stem cells. XbaI cleavage sites are marked by an "X." Red line indicates probe used for Southern blotting to assess targeting of ES cell colonies. Properly targeted ES cells generated a 9.5kb XbaI fragment; the wild type XbaI fragment was 12.5kb. B. Greater than 90% of *Tmem16a* null pups died within 9 days of birth. $Tmem16a^{+/+}$ n=19, $Tmem16a^{+/-}$ n=40, $Tmem16a^{-/-}$ n=22. C. *Tmem16a* null pups failed to thrive in the postnatal period. Data shown is mean weight +/- SEM. $Tmem16a^{+/+}$ n=7, $Tmem16a^{+/-}$ n=19, $Tmem16a^{-/-}$ n=8. D. Ventral view of whole mount tracheae from 3 day-old (P3) wild type and $Tmem16a^{-/-}$ pups stained with alcian blue to reveal tracheal cartilage rings. Gaps are observed along the ventral aspect of mutant tracheae. Transverse sections of newborn $Tmem16a^{-/-}$ trachea stained with alcian blue and eosin demonstrated multiple lateral cartilage elements with intervening epithelial evaginations instead of a single ventrolateral cartilage ring (compare E and F). Bar=100µm.

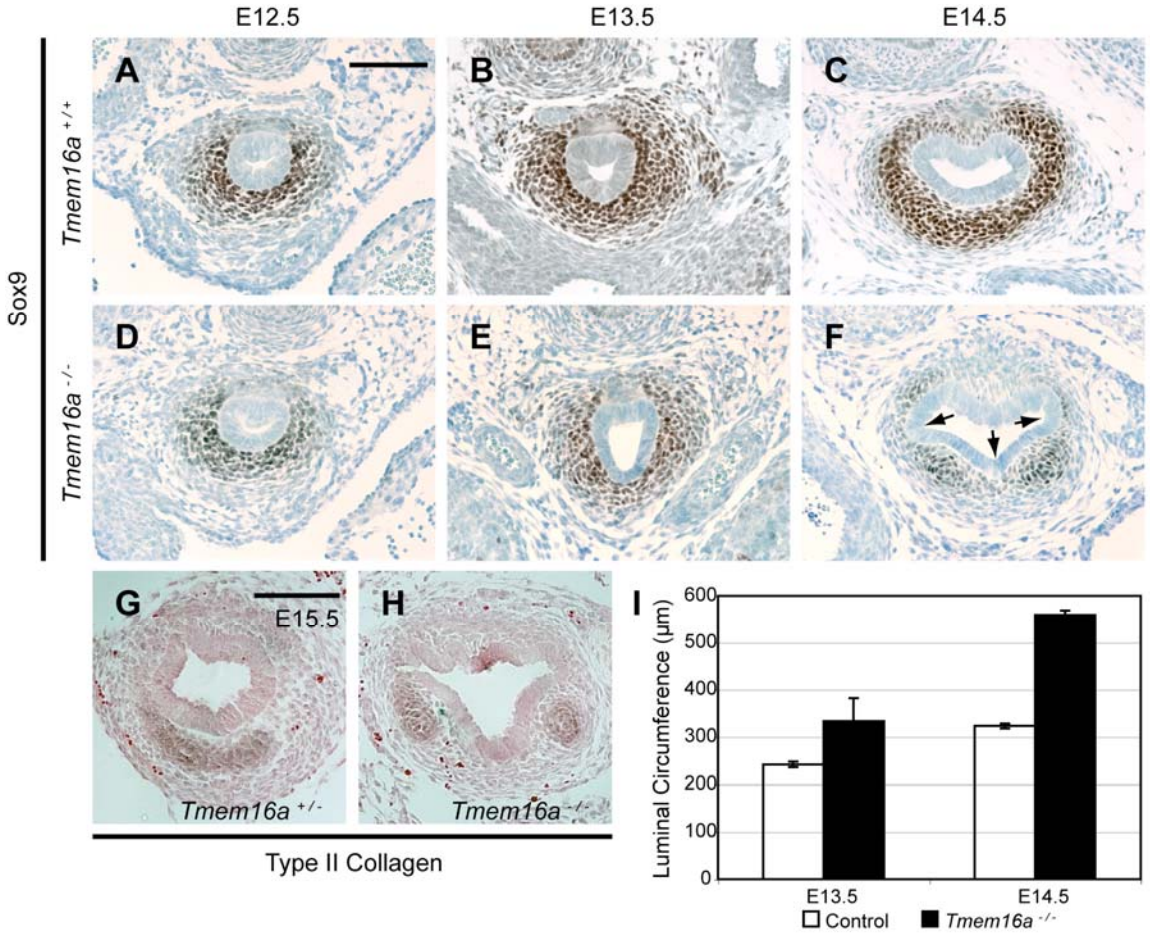

Figure 3-3. Tracheal lumen expansion in *Tmem16a* mutants redirects chondrogenesis in the surrounding mesenchyme. At E12.5 and E13.5, *Sox9*-expressing cells encircled the ventrolateral aspect of wild type (A,B) and *Tmem16a* mutant (D,E) tracheae. This distribution persisted in wild type tracheae at E14.5 (C). At E14.5, the epithelium of *Tmem16a* mutant trachea was thinner and evaginated into the surrounding mesenchyme (F, arrows mark evaginations disrupting mesenchymal *Sox9*-positive condensations). A single population of chondrocytes is present in the ventrolateral mesenchyme of the while type trachea on E15.5 as demonstrated by type II collagen immunohistochemistry (G). At E15.5, multiple chondrocyte populations were separated by epithelial evaginations in *Tmem16a* mutant tracheae (H). I. The tracheal lumen was expanded in *Tmem16a* mutants when compared to control lumens at E13.5 (*Tmem16a*$^{+/-}$) or E14.5 (*Tmem16a*$^{+/-}$ and *Tmem16a*$^{+/+}$ combined). Data shown is average of two measurements +/- s.e.m. for each data point. Scale bars=100µm.

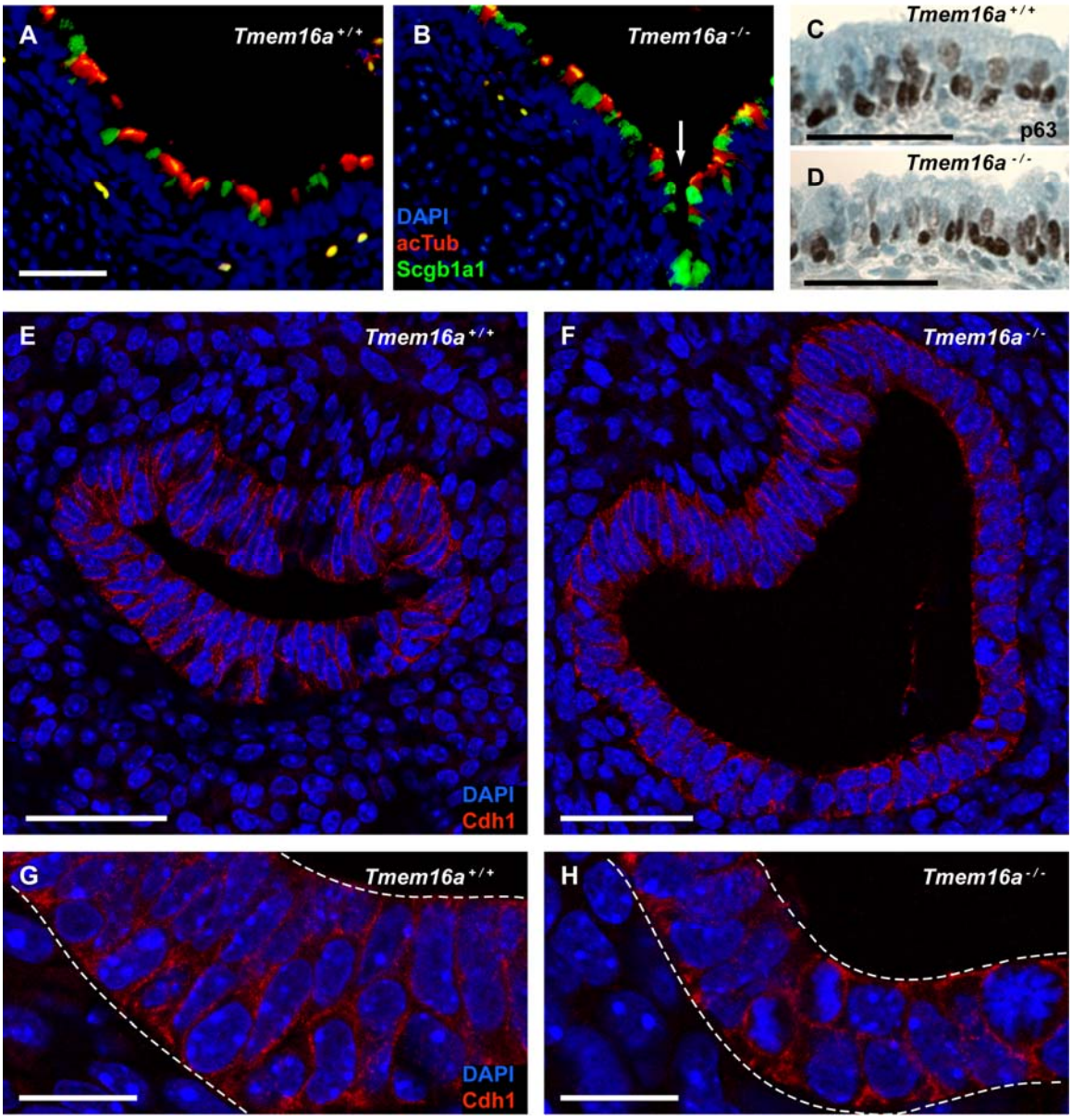

Figure 3-4. *Tmem16a* mutant epithelium contains Clara, basal, and ciliated cells, but lacks embryonic stratification. A. Acetylated α-tubulin and *Scgb1a1* reveal distribution of ciliated (red) and Clara cells (green) respectively in wild type newborn tracheal epithelium. B. Ciliated (red) and Clara cells (green) were present in *Tmem16a* mutant tracheal epithelium. However, only Clara cells and no ciliated cells were found in regions of epithelial evagination (arrow). C and D. Basal cells are identified by p63 immunohistochemistry in the epithelium of newborn wild type (C) and *Tmem16a* mutant (D) tracheae. E. *Cdh1* immunofluorescence and DAPI revealed epithelial cell membranes and nuclei, respectively, in wild type tracheal epithelium at E14.5. G. In wild type, the epithelium comprised 2-3 layers of cells. F. *Cdh1* immunofluorescence reveals a thinner epithelium in *Tmem16a* mutant tracheae at E14.5 with aberrant stratification (1-2 cell layers thick) and an expanded tracheal lumen. G and H are increased magnification of E and F. Dashed lines delineate the epithelial layer. Scale bars A-D=50μm; E,F=48μm; G-H=16μm.

CHAPTER 4
THE TMEM16 FAMILY OF PROTEINS

Members of the TMEM16 family of proteins characteristically contain eight predicted transmembrane domains with C- and N-termini facing the cytoplasm and a C-terminal domain of unknown function (DUF590 InterPro accession number IPR007632) (Katoh and Katoh, 2005) (Mizuta et al., 2007). One exception might be TMEM16G that is predicted to have 7 transmembrane domains (Bera et al., 2004). Very little is known about the *in vivo* expression patterns and functions of these genes. We have generated expression data for several murine TMEM16 genes and that data is reported here. Interestingly, we show that the expression of *Tmem16a* and *Tmem16g* overlap in multiple tissues. Although the precise functions of these proteins are unknown, at least three of the members of this family, TMEM16A, TMEM16E and TMEM16G, have influences on cell morphology (see Chapter 3 of this dissertation, (Tsutsumi et al., 2004), and (Das et al., 2007)).

Invertebrate TMEM16 Proteins

A single homolog, IST2, is found in the genome of the budding yeast Saccharomyces cerevisiae. In a high throughput screen of single gene mutations, IST2 mutants were shown to have a slightly increased tolerance to elevated concentrations of environmental NaCl (Entian et al., 1999). IST2 transcripts (and mRNAs from at least 23 other genes) are transported to the daughter cell during budding (Takizawa et al., 2000). In the daughter cell, IST2 is incorporated into the plasma membrane independently of the classical secretory pathway (Takizawa et al., 2000). An ancestral form of TMEM16 might therefore function at the plasma membrane to maintain osmotic homeostasis and is distributed asymmetrically during cell division.

Axs is one of four TMEM16 homologs reported in Drosophila melanogaster (Kramer and Hawley, 2003). AXS localizes to the endoplasmic reticulum and is recruited to the assembling

spindle microtubules of female meiotic germ cells. Furthermore, females expressing a mutant *Axs* cDNA in the germline exhibit abnormal spindle formation and an increase in the frequency of X chromosome nondisjunction (Kramer and Hawley, 2003).

Vertebrate TMEM16 Proteins

Ten paralogs of the TMEM16 family are predicted in humans and mice: *Tmem16a-h*, *Tmem16k*, and *Trp53i5* (Tmem16h is identified in (Katoh and Katoh, 2005) and others are reviewed in (Galindo and Vacquier, 2005)). The remainder of this chapter will summarize what is known about the expression and functions of the vertebrate TMEM16 family members. In collaboration with Amel Gritli-Linde (Department of Oral Biochemistry, Sahlgrenska Academy at Göteborg University, Sweden), we have characterized expression of *Tmem16a*, *Tmem16c*, *Tmem16f, Tmem16h* and *Tmem16k* during craniofacial development. This data is summarized in Appendix B but is not part of this dissertation.

Tmem16a

TMEM16A in cancer

Gastrointestinal stromal tumors are currently diagnosed based on activating mutations in the *KIT* tyrosine kinase receptor (West et al., 2004). These tumors are responsive to treatment with the receptor tyrosine kinase inhibitor imatinib mesylate. Unfortunately, a portion of GISTs is not immunoreactive for KIT despite oncogenic mutations therein. In addition, some GISTs harbor mutations in the *PDGFRA* and might also respond to imatinib mesylate treatment, but cannot be diagnosed by KIT immunoreactivity. Human *TMEM16A* was first identified in a cDNA microarray designed to characterize the expression profiles of different soft tissue tumors (Nielsen et al., 2002). In a subsequent tissue microarray study, 98% of GISTs were positively identified with a TMEM16A antiserum (*TMEM16A* was named *DOG1* in this study, Discovered on GIST-1) (West et al., 2004). Even those GISTs immunonegative for KIT were identified by

TMEM16A immunoreactivity and so TMEM16A is currently under investigation as a diagnostic and therapeutic tool for GISTs (Espinosa et al., 2008).

Human *TMEM16A* is found at chromosomal location 11q13, a region frequently amplified in a variety of carcinomas including those of the mouth, head, neck, esophagus, lung, bladder, and breast (Huang et al., 2006). Historically, 11q13 studies focused on two genes, cyclin D1 and cortactin, because of their known cellular functions and high levels of expression in tumors (Schuuring, 1995). The upregulation of *TMEM16A* expression has recently been shown to precede the amplification of this region in many oral squamous cell carcinoma primary tumors and cell lines, indicating that this gene might also have a function in the progression of 11q13 amplified tumors (Huang et al., 2006).

Expression of murine *Tmem16a*

Despite the clinical relevance of *TMEM16A*, very little is known about the mouse ortholog of this gene. We identified murine *Tmem16a* as a gene expressed specifically in the zone of polarizing activity during mouse limb development (Chapter 2 of this dissertation)(Rock et al., 2007). Another microarray experiment demonstrated a downregulation of *Tmem16a* in Runx2 null humeri at E14.5 (Hecht et al., 2007). That study also showed *Tmem16a* expression in the periosteum of the humeri of wild type mice.

We performed RNA *in situ* hybridizations on cryosections and whole mouse embryos at various developmental stages to determine the *in vivo* expression pattern of *Tmem16a*. *Tmem16a* was widely expressed at all stages examined (E10.5-E18.5) and there is no apparent bias of *Tmem16a* expression toward cells of any particular origin or fate.

At E10.5, *Tmem16a* expression was detected in the foregut endoderm (Figure 3-1A), and the mesenchyme of the mid- and hindgut (data not shown). At E12.5, expression was robust in the mesenchyme of the developing stomach (Figure 4-1A) and the mesenchyme surrounding the

esophagus (Figures 3-1D and 4-1A). This mesenchymal esophageal expression continued on E14.5 (Figure 4-1B,C), E15.5 (Figure 4-1D) and E16.5 (Figue 4-1H). Lower levels of *Tmem16a* expression were detected in the esophageal epithelium at E16.5 (Figure 4-1H).

Other sites of epithelial *Tmem16a* expression included the lung (Figures 3-1B,C, 4-1H, and 5-1), trachea (Figures 3-1, 4-1, and 5-1A,B), thymus (Figure 4-1C), vibrissae (Figure 4-1G), submandibular salivary gland (Figure 4-1J) and the lacrimal glands (Figure 4-1K). It is interesting to note that several of these epithelial structures are branched. In addition, specialized sensory epithelia expressed *Tmem16a*. These sites of expression included the retina (Figure 4-1E), the inner ear in the presumptive organ of Corti (Figure 4-1F), and the olfactory epithelium (data not shown).

Tmem16a expression was previously reported in the periosteum of the humerus at E14.5 (Hecht et al., 2007). We detected *Tmem16a* expression in the periostea of a number of bones including the basioccipital at E15.5 (Figure 4-1D) and the scapula and vertebrae at E16.5 (Figure 4-1I). The mesenchyme around the larynx and rostral trachea expressed *Tmem16a* at E14.5 (Figure 4-1B,D). This mesenchyme undergoes chondrogenesis to form the persistent cricoid and thyroid cartilages. Also of mesodermal origin, the walls of blood vessels, including the aorta, expressed *Tmem16a* (Figure 4-1A,C,H).

Tmem16c

The apical ectodermal ridge (AER) of the vertebrate limb bud produces members of the fibroblast growth family of proteins that are essential for outgrowth of the limb (Boulet et al., 2004; Sun et al., 2002). We generated an antisense probe to detect *Tmem16c* transcripts in mouse embryos. Expression of *Tmem16c* was observed specifically in the AER of the mouse limb by whole mount RNA *in situ* hybridization. *Tmem16c* expression was also detected in the somites at E10.5 by whole mount RNA *in situ* hybridization. Preliminary section RNA *in situ*

hybridizations suggest that *Tmem16c* is expressed in the epithelium of the gut at E12.5, but the specificity of this result must be confirmed.

Tmem16e

Gnathodiaphyseal dysplasia is a human disease characterized by bone fragility and cemento-osseous lesions of the jawbone (Tsutsumi et al., 2004). *TMEM16E* was *identified* as a potential genetic determinant of gnathodiaphyseal dysplasia by linkage analysis (TMEM16E is also called *GDD1*- gnathodiaphyseal dysplasia 1). Initially, two affected families with missense mutations in a conserved cysteine of *TMEM16E* were characterized (Tsutsumi et al., 2004). This is the only member of the TMEM family that has been associated with a human disease other than cancer.

An initial characterization of expression in adult mouse and human tissues demonstrated highest levels of *TMEM16E* expression in skeletal muscle and several bones including the calveria, femur, and mandible (Tsutsumi et al., 2004). Expression of murine *Tmem16e* was shown to increase during skeletal muscle differentiation in culture and decrease during osteoblast differentiation from a mesenchymal precursor cell line (Tsutsumi et al., 2005). Transfection of an epitope-tagged *hTMEM16E* construct resulted in localization of the tag to the endoplasmic reticulum. Interestingly, transfection of the tagged gnathodiaphyseal dysplasia-causing (mutant) alleles resulted in an abnormal rounded cell morphology and a decrease in adhesion (Tsutsumi et al., 2004).

The expression of *Tmem16e* was recently characterized in detail during mouse development (Mizuta et al., 2007). Between E9.5 and E11.5, *Tmem16e* expression was reported in the myotomal compartment of the somite. At E12.5, expression was detected in skeletal muscle progenitors in the limb bud and the perichondrium of the vertebral bodies. In addition, *Tmem16e* expression was detected in the intervertebral disks along the entire rostrocaudal axis.

At E14.5, *Tmem16e* expression was detected in the perichondria of the developing tarsals/carpals and phalanges. Immunohistochemistry with an antibody recognizing TMEM16E demonstrated protein in the long bones of the limbs that was not detected at the RNA level. Hypertrophic chondrocytes, osteoblasts, and articular chondrocytes demonstrated TMEM16E immunoreactivity in adult mice, but TMEM16E was restricted to prehypertrophic chondrocytes in late embryonic bones (Mizuta et al., 2007).

This antibody also showed the presence TMEM16E in differentiated, multi-nucleated myotubes but not in mononuclear myoblasts in culture. Furthermore, increased levels of TMEM16E were detected in the skeletal muscles of mice deficient for dystrophin (Mizuta et al., 2007). In cardiac muscle, TMEM16E was found in both the cytoplasm and within the sarcolemma. Fractionation experiments with this antibody demonstrated highest levels of TMEM16E protein in intracellular membranes of cultured myotubes (Golgi apparatus, secretory vesicles, endosomes, endoplasmic reticulum and trans-Golgi network) with lower levels on the plasma membrane (Mizuta et al., 2007).

Tmem16f

A gene trap allele of *Tmem16f*

In contrast to targeted deletions made in embryonic stem (ES) cells such as the one we constructed for *Tmem16a*, mutations generated by random insertions in ES cells are now available from public resources for a number of genes. This approach is known as gene trapping. To generate a gene trapped ES cell line, an ES cell culture is either electroporated with a promoterless selection cassette (such as neomycin resistance) or transduced with a retrovirus carrying a selection cassette. In both cases, random integration of the transgenic construct into the genome will render its expression under the control of the endogenous cis-acting elements. Translation will fuse the transgene with any upstream gene product from the endogenous locus.

In some instances, depending on the location of insertion within a gene, this will produce hypomorphic (less functional) or null (nonfunctional) allele of the gene in which the insertion took place. The sites of such integrations are usually determined by 5' RACE and published in databases for distribution (http://www.genetrap.org/).

We obtained a gene trapped allele of murine *Tmem16f*, *Tmem16f*^{RRF355} (Figure 4-3A,B). Southern blot of ES genomic DNA confirmed integration of a β-galactosidase/neomycin fusion construct (β-geo) had occurred in an intron of *Tmem16f* (Figure 4-3C). These cells were injected into blastocysts to generate chimeric animals. Germline transmission of the gene trapped allele was confirmed by PCR on tail DNA samples from the progeny of these chimeras. Embryos heterozygous for the gene trapped allele (*Tmem16f*$^{RRF355/+}$) were generated by breeding chimeras to wild type mice and sacrificing dams during pregnancy.

The expression of β-galactosidase is presumably under the control of the *Tmem16f* promoter and enhancer elements in *Tmem16f*$^{RRF355/+}$ mice. Therefore, visualizing β-galactosidase distribution in these embryos is an indirect method of detecting the temporospatial pattern of *Tmem16f* expression. Using the chromogenic substrate X-gal, we determined the distribution of β-galactosidase in E14.5 *Tmem16f*$^{RRF355/+}$ mice.

Developmentally speaking, bones arise by one of two mechanisms (reviewed in (de Crombrugghe et al., 2001)). During intramembranous ossification, which occurs in many bones of the head, mesenchymal condensations differentiate directly into osteoblasts and deposit bone matrix. Endochondral ossification produces most bones of the body including the long bones of the limbs. In this process, mesenchymal conensations differentiate into cartilage intermediates that ultimately die and are invaded by osteoblasts and vascularized (reviewed in (Provot and Schipani, 2005)).

X-gal staining *Tmem16f*$^{RRF355/+}$ embryos on E14.5 suggested that *Tmem16f* was expressed in a number of developing bones of the head including the maxilla, mandible, parietal, and zygomatic bones (Figure 4-4A). These bones arise from intramembranous ossification and do not involve a cartilage intermediate. Also in the head, X-gal staining was detected in the mesenchymal component of the submandibular gland (where we previously detected transcription of Tmem16a (Figures 4-4A and 4-1J).

Interestingly, the centers of ossification in the long bones of the fore- and hindlimbs also exhibited β-galactosidase activity on E14.5 (Figure 4-4B). These bones arise by the process of endochondral ossification. Expression of *Tmem16f* was also detected in the developing ribs on E14.5 (Figure 4-4C). *Tmem16f* expression in the submandibular gland and both types of bones, those arising by intramembranous ossification as well as those arising by endochondral ossification, suggests that *Tmem16f* might have a general role in mesenchymal organization or differentiation. Many bones did not exhibit *Tmem16f* expression detectable by X-gal staining (e.g. the phalanges) but might express other members of the TMEM16 family of proteins with similar functions (Figure 4-4B and data not shown).

It is not known if *Tmem16f*^{RRF355} is a null or hypomorphic allele of *Tmem16f*. This is a possibility since the insertion of the β-galactosidase transgenic construct includes a termination codon and polyadenylation sequence 3' of β-geo (Figure 4-3B). Insertion of this construct should result in the termination of translation before 6 out of the 8 predicted transmembrane domains of TMEM16F. This termination is also 5' of the DUF590 domain that is conserved in all of the TMEM16 proteins. In the future, this allele might be used to determine the function of *Tmem16f* in vertebrate development by generating *Tmem16f*$^{RRF355/RRF355}$ mice.

RNA *in situ* hybridization analysis of *Tmem16f* expression

We performed section RNA *in situ* hybridizations on mouse cryosections to further characterize the expression of *Tmem16f* in vivo. Interestingly, *Tmem16f* expression overlapped in a number or sites with the expression of *Tmem16a*.

On embryonic day 16.5, expression of *Tmem16f* was detected in the periosteum of the vertebral bodies (Figure 4-5A). This expression has been described for *Tmem16a* (Figure 4-1I) and *Tmem16e* (Mizuta et al., 2007). Another site of overlapping expression of *Tmem16f* and *Tmem16a* was the submandibular gland (compare figures 4-5B and 4-1J). The epithelium and lamina propria of the larynx expressed moderate levels of *Tmem16f* at this stage as did the epithelium and developing muscularis externa of the esophagus (Figure 4-5A). The dorsal root ganglia expressed high levels of *Tmem16f* at E16.5 (Figure 4-5A). A number of skeletal muscles and a subset of cells in the ventral spinal cord demonstrated *Tmem16f* expression at E16.5 (Figure 4-5A).

Tmem16f expression was detected by RNA *in situ* hybridization on E14.5 in the epithelium of the lung and at lower levels in the mesenchyme of the lung (Figure 4-5C). At this stage, *Tmem16a* expression is apparently more proximally biased in the epithelium of the lung while *Tmem16f* expression is detected more distally (compare Figures 5-1E,F and 4-5C). *Tmem16f* transcripts were also detected in the periostea of the vertebral bodies at E14.5 (Figure 4-5C).

Tmem16g

A microarray screen (Kiessling et al., 2005) and an *in silico* screen (Bera et al., 2004), both designed to identify prostate-specific transcripts, identified *TMEM16G* (named *D-TMPP* and *NGEP*) as a gene transcribed specifically in the prostate. One group went on to characterize two transcripts in both normal and cancerous prostate epithelial tissue and cell lines (Bera et al., 2004). Interestingly, they showed that a short transcript was localized intracellularly while a

longer transcript was localized to the plasma membrane. In contrast to the eight predicted transmembrane domains of other TMEM16 family members, TMEM16G is predicted to comprise seven. This arrangement necessitates that one terminus be extracellular.

A polyclonal TMEM16G antibody was generated and used to localize TMEM16G to the plasma membranes of cancer cells (LNCaP) transfected with a cDNA construct of the long *TMEM16G* transcript (Das et al., 2007). TMEM16G was also detected with this antibody in the epithelia of normal and malignant prostates. The plasma membrane localization of TMEM16G was most intense at regions of cell:cell contract. When *TMEM16G* was transfected into LNCaP cells, large clumps of cells formed and the cellular morphology of those cells not in clumps was drastically altered (cells became round and less spread out) (Das et al., 2007).

Experimental Procedures

RNA *in situ* Hybridization

RNA *in situ* hybridizations were performed according to an adapted standard protocol (Nieto et al., 1996). The generation of the antisense riboprobes used is summarized in Appendix C.

Generation of *Tmem16f*$^{RRF355/+}$ mice

Gene trapped embryonic stem cell clone RRF355 was purchased from Bay Genomics (San Francisco, CA http://www.genetrap.org/). These cells were expanded according to standard culture technique. Targeting of the Tmem16f locus was confirmed by Southern blot. Briefly, RRF355 and wild type CJ-7 ES cell genomic DNA preparations were independently digested with EcoRV or XbaI and electrophoresed on agarose gels. The digested genomes were then transferred to nitrocellulose membranes and probed with a radioactive probe corresponding to a region of the *Tmem16f* genomic sequence near the reported site of insertion (synthesized from Harfe lab plasmid BH198).

Once insertion of the transgenic construct into *Tmem16f* was confirmed, RRF355 ES cells were injected into blastocysts to generate chimeric offspring. These chimeras were bred to wild type females to generate *Tmem16f*$^{RRF355/+}$ mice that were identified by PCR using the oligonucleotides listed in Appendix A.

X-gal Visualization of β-galactosidase

To perform X-gal visualization β-galactosidase distribution in vivo, embryos were isolated on E14.5 and fixed overnight at 4ºC in 0.2% PFA. Embryos were washed in PBS and concentrated lacZ rinse buffer prior to staining in X-gal according to standard protocol at room temperature for 16 hours.

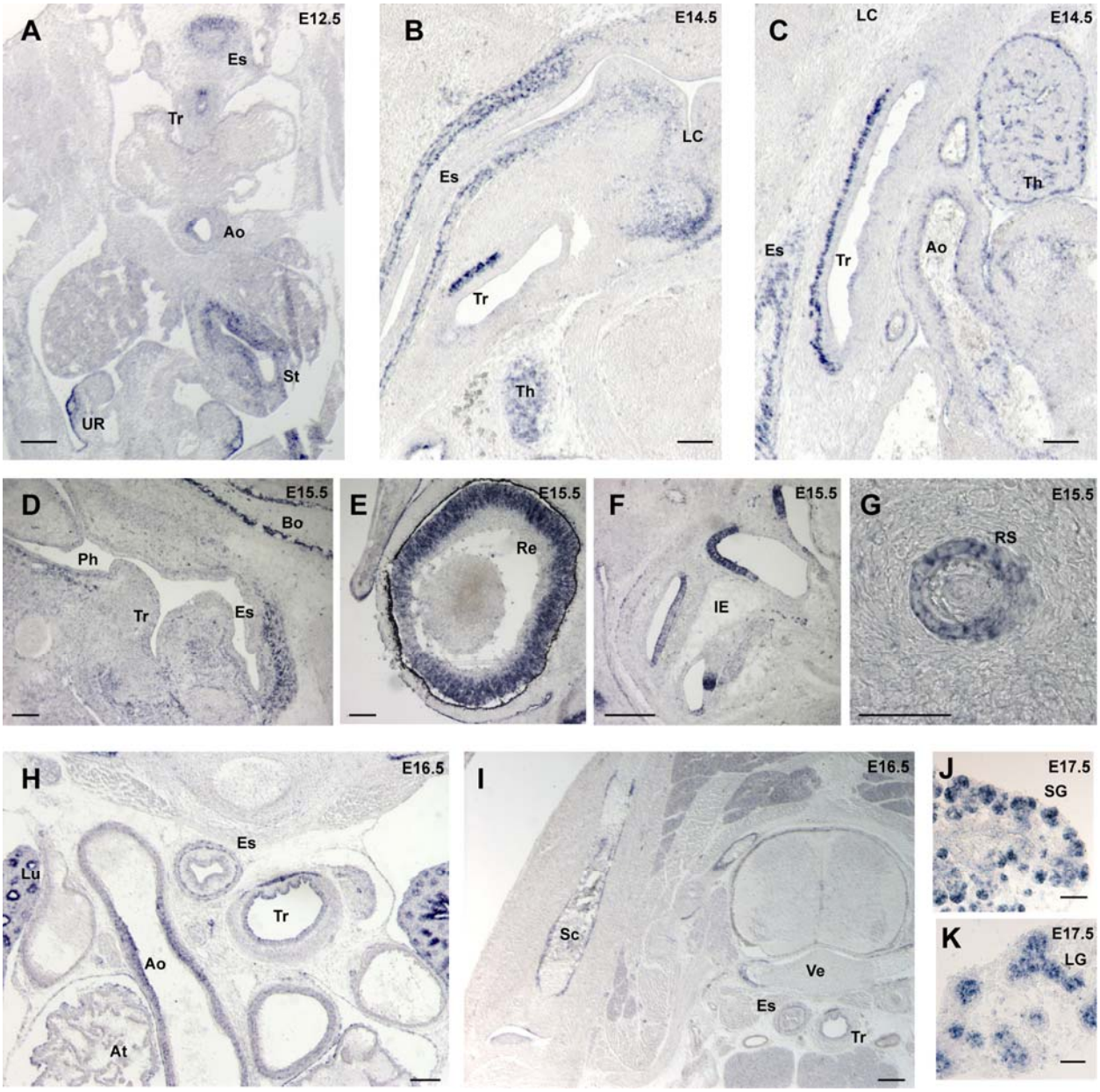

Figure 4-1. *Tmem16a* is widely expressed during mouse development. Abbreviations: Es, esophagus; Tr, trachea; Ao, aorta; St, stomach; UR, urogenital ridge; LC, laryngeal cartilages; Th, thymus; Ph, pharynx; Bo, basioccipital bone; Re, retina; IE, inner ear; RS, root sheath; Lu, lung; At, atrium; Sc, scapula; Ve, vertebra; SG, submandibular gland; LG, lacrimal gland. Scale bars: A-E,H=100µm, F,G,J,K=50µm, I=200µm.

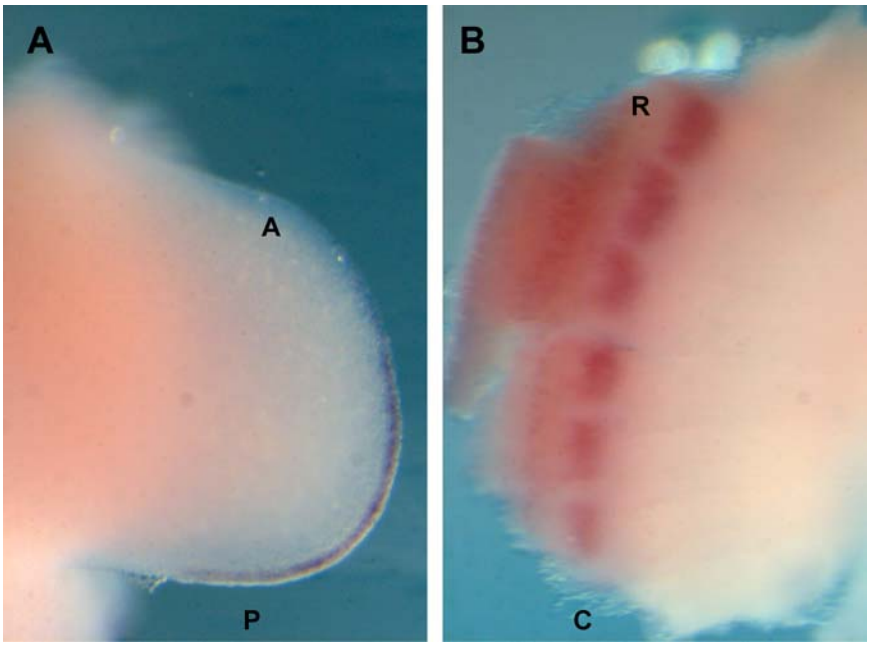

Figure 4-2. *Tmem16c* is expressed in the mouse embryo. A. Whole mount RNA *in situ* hybridization showing *Tmem16c* expression in the apical ectodermal ridge at E10.5 B. RNA *in situ* hybridization showing *Tmem16c* expression in the somites and neural tube on E10.5. Abbreviations: A, anterior; P, posterior; R, rostral; C, caudal.

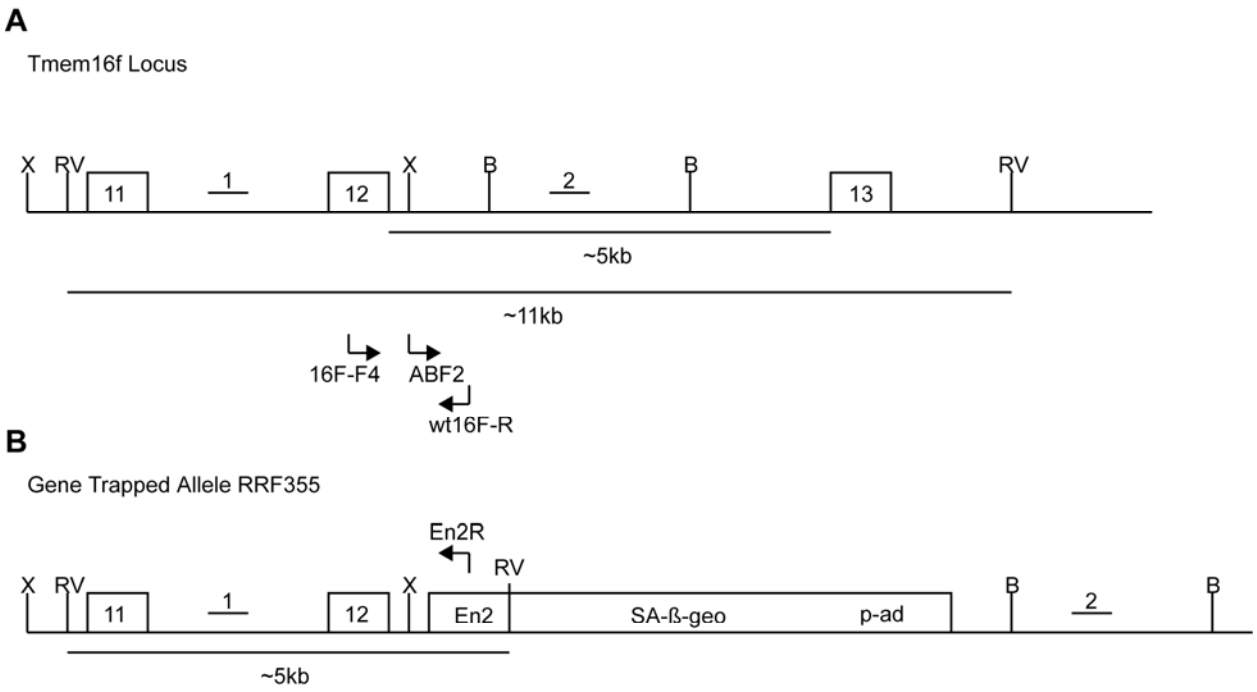

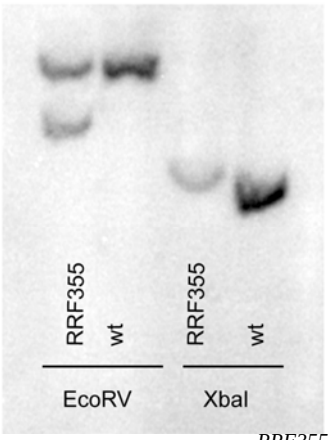

Figure 4-3. *Tmem16f*$^{RRF355/+}$ is a gene trapped allele of *Tmem16f*. A. A portion of the endogenous murine *Tmem16f* locus. B. Gene trapped allele *Tmem16f*$^{RRF355/+}$ showing insertion of β-geo in the intron between exons 12 and 13. C. Southern blot of wild type (CJ.7) and *Tmem16f*$^{RRF355/+}$ embryonic stem cell genomic DNA digested with EcoRV or XbaI and probed with "probe 1." A second, smaller band in the *Tmem16f*$^{RRF355/+}$ lane digested with EcoRV suggested the introduction of an EcoRV cleavage site in this fragment by insertion of the β-geo cassette. Probe 1 is Harfe lab plasmid BH198. Primers used to genotype alleles are shown by arrows and listed in Appendix A. Abbreviations: X, XbaI cleavage site; RV, EcoRV cleavage site; B, BamHI cleavage site; En2, engrailed 2 intron sequence included in selection cassette; SA-β-geo, splice acceptor and fusion of coding sequences of neomycin resistance and β-galactosidase; p-ad, poly-adenylation.

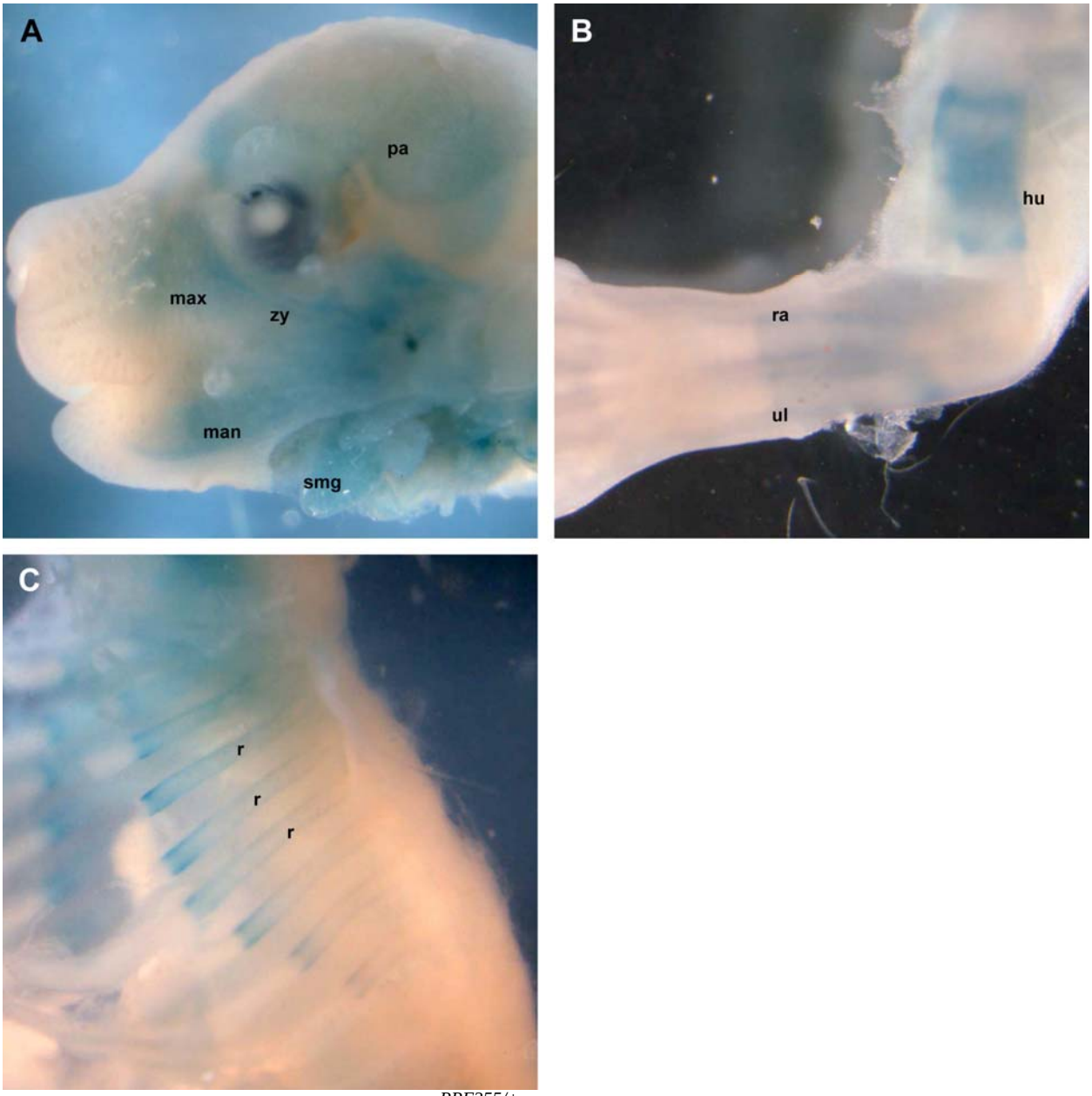

Figure 4-4. X-gal staining of *Tmem16f*$^{RRF355/+}$ embryos at E14.5. A. β-galactosidase activity was detected in bones of the head forming via intramembranous ossification and the submandibular gland. B. β-galactosidase activity was detected in the radius, ulna, and humerus developing via endochondral ossification. C. The ribs of E14.5 *Tmem16f*$^{RRF355/+}$ demonstrated β-galactosidase activity at E14.5. Abbreviations: par, parietal; max, maxilla; zyg, zygomatic; man, mandible; smg, submandibular gland; hu, humerus; ra, radius; ul, ulna; r, rib.

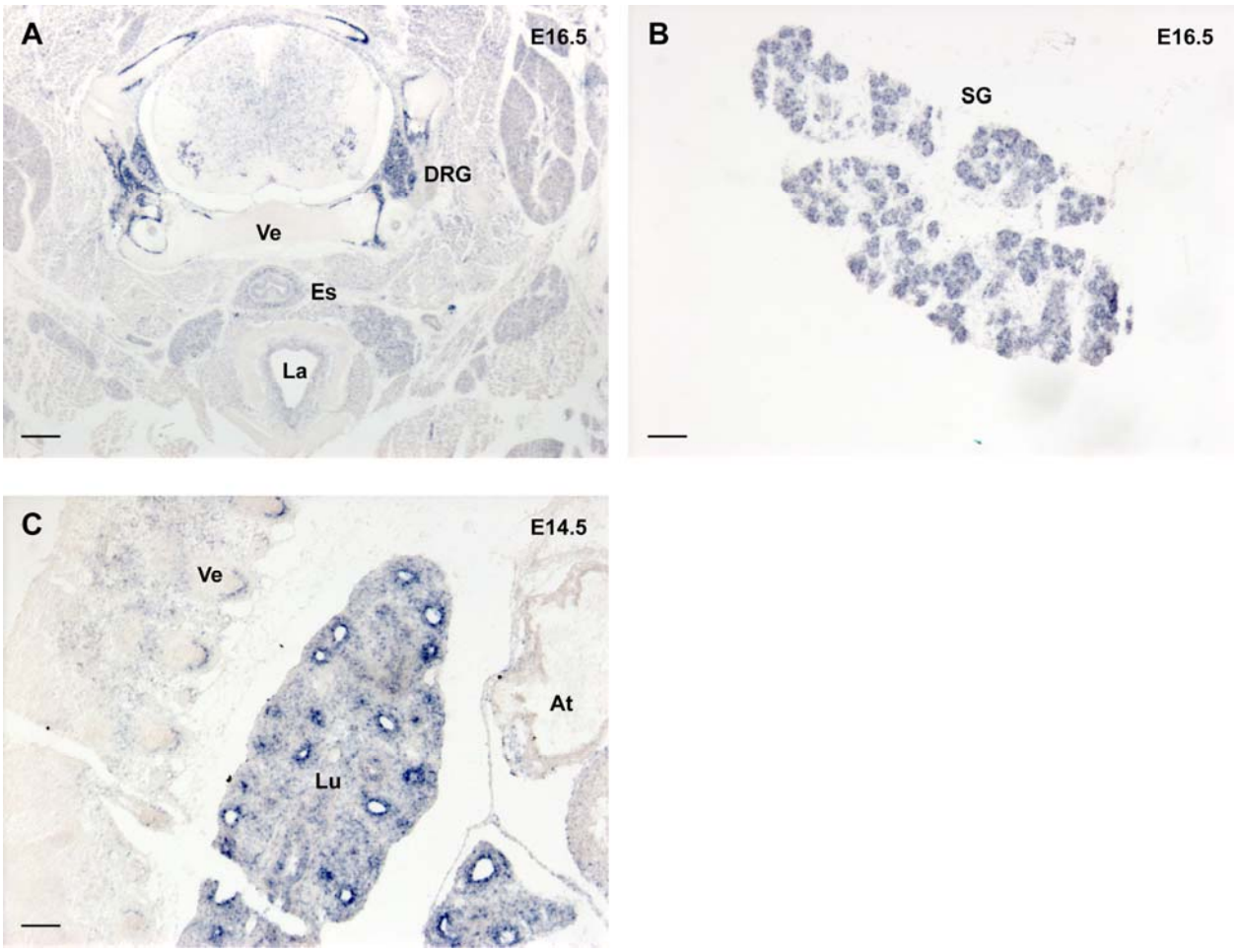

Figure 4-5. *Tmem16f* expression in the mouse embryo detected by RNA *in situ* hybridization. A. *Tmem16f* expression in a transverse cryosection of an E16.5 mouse embryo. B. Cryosection of mouse submandibular gland on E16.5 showing expression *Tmem16f*. C. *Tmem16f* expression at E14.5. Abbreviations: Ve, vertebral body; DRG, dorsal root ganglion; Es, esophagus; La, larynx; SG, submandibular gland; Lu, lung; At, atrium. Scale bars A=200µm, B,C=100µm.

CHAPTER 5
IMPAIRED POSTNATAL LUNG DEVELOPMENT IN *TMEM16A* MUTANT MICE

Introduction

The mammalian lung is intricately patterned during development as one strategy to efficiently exchange the volumes of gases necessary to support metazoan life on land. In mice, lung development is initiated approximately 9.5 days after conception and continues well into postnatal life as the surface area for gas exchange increases through the process of alveolarization and the lung responds to environmental cues (Warburton et al., 2000) (Burri, 2006).

Two epithelial buds evaginate from the ventral foregut endoderm and grow into the surrounding splanchnic mesenchyme around embryonic day (E) 9.5 (Warburton et al., 2000). These epithelial buds and surrounding mesenchyme signal to one another in a series of iterative branching events during the pseudoglandular stage of lung development (E9.5-E16.5) that result in a tree-like organ with larger conducting airways rostrally and successively smaller airways at the periphery. Branching morphogenesis continues in mice until the most distal epithelial buds dilate into terminal saccules during the canalicular and saccular stages of lung development (E16.5-E17.5 and E15.7-P5, respectively). The mesenchyme is reduced and the epithelium flattens in intimate juxtaposition to a capillary network to facilitate gas exchange. In both mice and humans alveolarization occurs postnatally (P5-P30 in mice) as septae subdivide these terminal saccules into hundreds of millions of alveoli (Burri, 2006).

The cyanotic appearance of *Tmem16a* null embryos and the expression of *Tmem16a* in the developing lung led us to speculate that there might be a lung defect in *Tmem16a* mutants (see Chapter 3 of this dissertation). We found that *Tmem16a* mutant lungs failed to complete the process of alveolarization after birth. By P3, those mutants surviving demonstrated an

emphysematous phenotype characterized by distal airway enlargement. However, malnutrition has been reported to cause emphysema in humans and animal models (reviewed in (Kalenga, 1997)) and so the emphysema observed in *Tmem16a* mutants might be a consequence of their failure to thrive. We did not observe any defects in differentiation in *Tmem16a* mutant lungs.

Results

Tmem16a is Expressed in a Dynamic Pattern in the Developing Murine Lung

As described previously in this dissertation, whole mount and section RNA *in situ* hybridizations detected *Tmem16a* expression in the epithelium of the trachea and the primary lung buds from E10.5-E12.5 (Figures 3-1 and 5-1A,B). Expression was observed in the proximal conducting airways at E11.5 and E12.5, but was absent from the distal tips of the epithelial buds. Whole mount RNA *in situ* hybridization revealed a similar pattern of *Tmem16a* expression in E13.5 lungs (Figure 5-1C,D).

To determine the expression pattern of *Tmem16a* in highly branched E14.5 lungs, we performed RNA *in situ* hybridization on cryosections of wild type lungs. At this stage, *Tmem16a* expression was detected most strongly in the epithelium of branchpoints and the epithelium between branchpoints and the most distal epithelium of the buds (Figure 5-1E,F). Low levels of *Tmem16a* expression were occasionally observed in the epithelium of more proximal conducting airways but expression was never observed in the most distal dilated terminal buds.

In stark contrast to earlier stages of development, RNA *in situ* hybridization on E18.5 lung cryosections revealed *Tmem16a* expression biased to the most distal epithelium (Figure 5-1G,H). At high magnification, it is apparent that a subset of distal epithelial cells expresses *Tmem16a* at high levels (Figure 5-1I). *Tmem16a* expression was not detected in the mesenchyme of the lung at any stage examined.

Tmem16a Mutant Lungs Fail to Develop Alveoli

After birth, the terminal saccules of the lung undergo the process of alveolarization in order to increase the surface area available for gas exchange (Prodhan and Kinane, 2002) (Burri, 2006). At birth, the lungs from *Tmem16a* mutants were histologically indistinguishable from those of wild type animals (compare Figure 5-2 A and D). This suggested that branching morphogenesis and the formation of terminal sacs had occurred normally in the absence of *Tmem16a*.

At P3, we noticed a thinning of the parenchyma in the lungs of *Tmem16a* mutants accompanied by a decrease in the number of septae (compare Figure 5-2B and E). Although most *Tmem16a* mutants die within 9 days of birth (see Chapter 3), those surviving 21 days exhibited a severe disruption in alveolar formation (compare Figure 5-2C and F). To determine the cause of this defect, we characterized apoptosis and proliferation in *Tmem16a* mutants before birth (at E18.5), but were unable to identify any change from the wild type condition. We observed an increase in apoptosis at P3 in mutant lungs, but reasoned that this might be secondary to their failure to thrive (data not shown). Caloric restriction in mice has been shown to trigger cell death in alveoli via a variety of pathways (Massaro et al., 2004).

Differentiation Is Not Affected in *Tmem16a* Mutant Lungs

The mature lung is reported to comprise at least 40 morphologically distinct cell types (Warburton et al., 1998). To further characterize the emphysematous defect we observed in *Tmem16a* mutant lungs, we immunohistologically characterized differentiation of the major cellular constituents of the lung. In the most distal airways of the lung, the alveoli, there exist two epithelial cell types. The squamous type I alveolar epithelial cells (AEC) are the primary sites of gas exchange and cover 95% of the alveolar surface area (Berthiaume et al., 2006). The cuboidal type II AECs, among other functions, synthesize and secrete pulmonary surfactant that

is essential to the normal physiology of the lung (Fehrenbach, 2001). In addition, at least a subpopulation of type II AECs is a progenitor population in the mature lung capable of transdifferentiation into type I AECs in response to injury (Evans et al., 1975).

To determine if type II AECs had a normal distribution in the lungs of *Tmem16a* mutants, we performed RNA *in situ* hybridizations with a riboprobe to the surfactant associated protein C (*Sftpc*) (Warburton et al., 2000). Newborn *Tmem16a* mutant and wild type lungs had similar distributions of *Sftpc*-expressing cells at all stages examined (Figure 5-3A-F). As alveolarization proceded, *Sftpc*-expressing cells in wild type and mutant lungs became localized to the corners of alveoli, consistent with published type II AEC distribution (Bhaskaran et al., 2007). Although the number of type II AECs at P8 and P15 is apparently lower in *Tmem16a* mutant lungs than wild type, this was possibly a function of a general decrease in parenchyma rather than a type II AEC-specific defect (Figure 5-3E,F). To address this possibility, we performed Northern blots with RNA from postnatal wild type and *Tmem16a* mutant lungs and did not observe a reduction in the amount of *Sftpc* RNA (data not shown).

T1α (also known as glycoprotein 38 or GP38) is a glycoprotein expressed at high levels on the membranes of type I AECs (Eblaghie et al., 2006). We used an antibody to T1α in order to identify this cell type. Type I AECs visualized by this method lined the lungs of both wild type and mutant newborn lungs (Figure 5-4A,B).

Nkx2.1 (also known as Titf1 or Ttf-1) is a homedomain transcription factor expressed in the lung and thyroid (both foregut endoderm derivatives) and parts of the brain (Minoo et al., 1999). Late in gestation and postnatally, Nkx2.1 is detected in the nuclei of distal epithelial cells of the lung (type I and type II AECs). We detected Nkx2.1 positive cells by immunohistochemistry in control and *Tmem16a* mutant lungs at E18.5 with similar distributions

and abundances (Figure 5-5A,B). Notably, the Nkx2.1 labeled nuclei in *Tmem16a* mutants were rounder than the oblong nuclei labeled in the wild type sample (compare Figure 5-5A and B). It is not presently clear if this is an artifact of tissue processing (i.e. inflation fixation, see Experimental Procedures) or a real consequence of TMEM16A deficiency in distal epithelial cells. The latter is an attractive possibility given the effect of TMEM16A on tracheal epithelial morphology (see Chapter 3) and the influence of TMEM16E and TMEM16G on cellular morphology (Das et al., 2007) (Tsutsumi et al., 2004). At P3, we detected fewer Nkx2.1 positive cells in the lungs of *Tmem16a* mutants (Figure 5-5C.D). Similarly to type II AECs, it is possible that this difference is attributable to a general decrease in lung parenchyma and is not specific to Nkx2.1-positive cells.

During the alveolar stage of lung development, a population of smooth muscle cells migrates into the nascent alveoli and synthesizes elastin, the primary component of the pulmonary extracellular matrix (Lindahl et al., 1997). The failure of this process in the absence of the PDGFRA results in a failure of alveolar septation. To localize this population of cells during terminal lung development of *Tmem16a* mutants, we performed RNA *in situ* hybridization with a probe for tropoelastin at P15. Although already emphysematous, tropoelastin-expressing cells were found in the alveoli of *Tmem16a* mutant lungs with relatively normal distribution (Figure 5-6B).

Gas exchange in the lung necessitates an intimate association between the alveoli and the capillary network. We used an antibody against PECAM-1 (platelet-endothelial cell adhesion molecule-1 or CD31) to immunofluorescently label endothelial cells in the lungs of *Tmem16a* mutants and wild type pups. The distribution of endothelial cells in the walls of the alveoli of *Tmem16a* mutants resembled that observed in wild type lungs at P7 (Figure 5-6C,D).

More proximally in the lung, other types of epithelial cells are found. These include the non-ciliated secretory Clara cells and ciliated columnar epithelial cells (Rawlins and Hogan, 2006). We observed a normal distribution of Clara cells in the proximal airways of *Tmem16a* mutants by immunolocalizing the most abundant secretoglobin they synthesize, *Scgb1a1* (also known as CC10 or CCSP) (Figure 5-6EF).

Discussion

Mammalian lung development occurs in four distinct stages (reviewed in (Warburton et al., 2000)). The rapid generation of millions of alveoli occurs primarily after birth in mice and humans and is essential to support life on land. A better understanding of this process will yield therapies for premature infants and might reveal unrecognized regenerative potential for emphysematous patients.

Tmem16a mutant mice surviving into the postnatal alveolar stage of lung development do not complete alveolar septation. This septation defect is not coupled with any defect in differentiation that we observed. Furthermore, we did not detect a prenatal change in proliferation or apoptosis of mutant lungs. It is possible that the postnatal failure to thrive of *Tmem16a* mutants contributes to their pulmonary emphysema. During World War II, physicians documented emphysema in starved humans and this phenomenon has been validated by a number of animal models (Kalenga, 1997). If the emphysema in *Tmem16a* mutants is coupled to their failure to thrive in the postnatal period, it is obvious that a number of other mutants with a similar combination of phenotypes warrant reevaluation.

The emphysema observed in *Tmem16a* mutants might be a direct consequence of (or at least partly attributable to) the removal of *Tmem16a* from the lung. One way to assess this possibility is through the generation of a conditional allele of *Tmem16a*. Using a pulmonary epithelium-specific Cre (Perl et al., 2002) in combination with such a conditional allele would

ablate *Tmem16a* specifically from the lung. Any defect observed in these animals would be the direct result of *Tmem16a*-deficiency in the lung; *Tmem16a* would be normally expressed in other tissues. It is worth noting that at least one other member of the TMEM16 family of proteins, TMEM16F, is expressed in the developing lung (Figure 4-5C). In the future, mice lacking multiple members of this family (that might have the same or similar functions) might contribute to the understanding of their functions in locations where they are coexpressed.

Experimental Procedures

Sample Collection and Preparation

The generation of *Tmem16a* mutants was described previously (see Chapter 3). Following sacrifice, lungs were dissected from wild type or *Tmem16a* mutant embryos or pups. For histological and immunohistochemical specimens, lungs were inflated with 4% paraformaldehyde to a transpulmonary pressure of 20cm H_2O for 30 minutes before fixation overnight at 4ºC in PFA and subsequent paraffin embedding according to a standard protocol. Samples used for RNA *in situ* hybridizations were harvested in DEPC-treated PBS, fixed in 4% PFA overnight at 4ºC, and embedded for cryosectioning according to a standard protocol. Samples used for PECAM immunofluorescence were fixed in a commercial zinc fixative (BD Biosciences, San Jose, CA) instead of PFA overnight at 4ºC prior to embedding in paraffin.

RNA *in situ* Hybridization

RNA *in situ* hybridizations were performed according to an adapted standard protocol (Nieto et al., 1996). The generation of the antisense riboprobes used is summarized in Appendix C.

Histology, Immunohistochemistry and Immunofluorescence

7µm sections were dewaxed and rehydrated. Hematoxylin and eosin was performed according to a standard protocol.

For immunohistochemistry and immunofluorescence, antigen retrieval was performed by microwaving samples in 10mM citric acid pH 6.0 for 20 minutes. For immunohistochemistry, endogenous peroxidases were blocked in 3% hydrogen peroxide. Primary antibodies used were: hamster anti-T1α (Developmental Studies Hybridoma Bank, used at 1:100), mouse anti-Nkx2.1 (Thermo Scientific, used at 1:50), rat anti-PECAM (BD Pharmingen, used at 1:500), and goat anti-CC10 (Santa Cruz Biotechnology, used at 1:100). T1α was visualized with TSA kit (Perkin Elmer) and metal-enhanced DAB (Pierce). Nkx2.1 was visualized with MOM kit (Vector Laboratories) and metal-enhanced DAB. Secondary antibodies used for immunofluorescence were Cy3-conjugated donkey anti-rat and Cy3-conjugated donkey anti-goat (Jackson Immunoresearch). Counterstains used were Richardson's Azure II (for T1α immunohistochemistry), eosin (for Nkx2.1 immunohistochemistry), and DAPI (Pierce Biotechnology, for immunofluorescence). Images were acquired using a Lecia DFC300 FX camera.

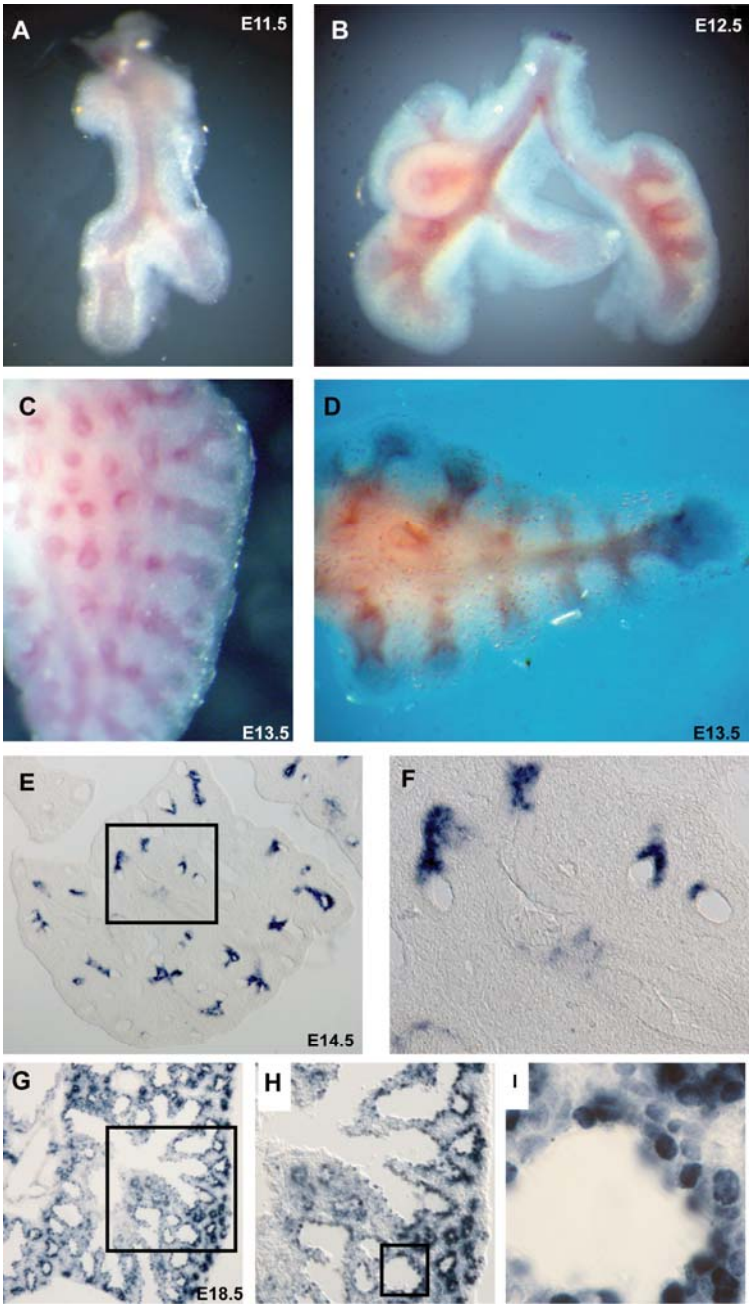

Figure 5-1. *Tmem16a* is expressed in the developing lung. Whole mount RNA *in situ* hybridizations showing *Tmem16a* expression at A. E11.5, B. E12.5, and C. and D. E13.5. Notice expression of *Tmem16a* in the proximal, conducting airway epithelium but not in the most distal tip epithelia. E. Section RNA *in situ* hybridization showing expression of *Tmem16a* in the lung epithelium but not in the most distal epithelium. F. Higher magnification of E. G. Expression of *Tmem16a* in the distal epithelium of E18.5 lungs. H. Higher magnification of G. I. Higher magnification of H.

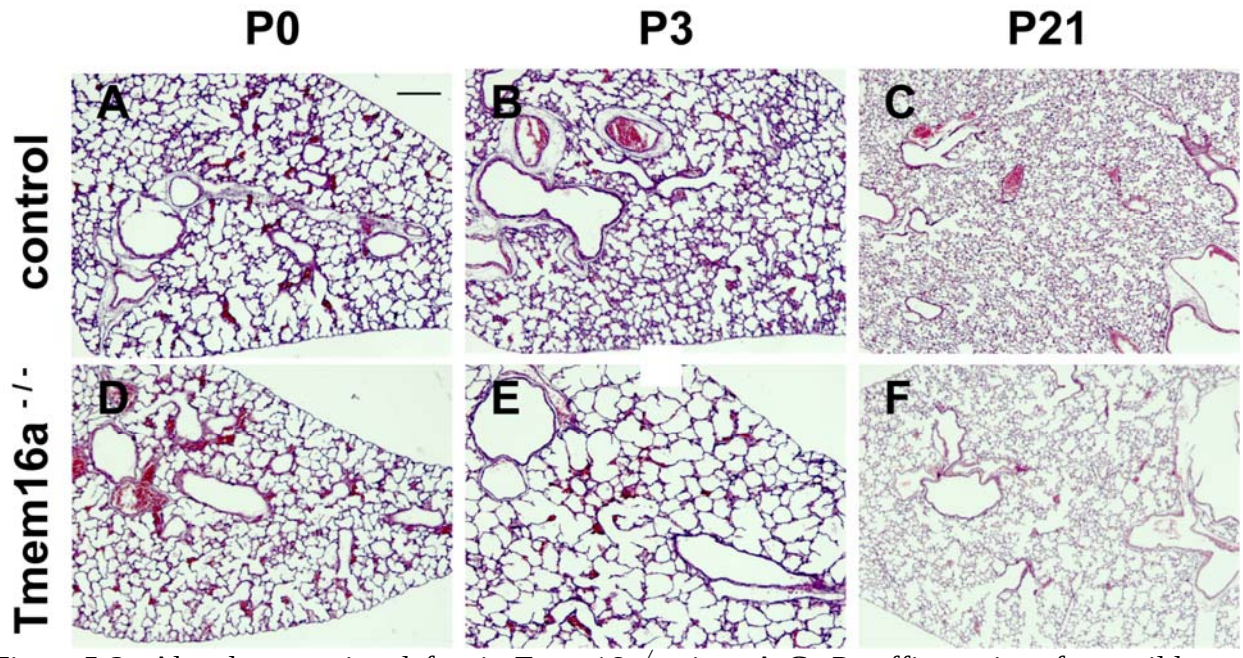

Figure 5-2. Alveolar septation defect in *Tmem16a*$^{-/-}$ mice. A-C. Paraffin sections from wild type or *Tmem16a*$^{-/+}$ lungs stained at A. P0, B. P3, and C. P21 with hematoxylin and eosin to demonstrate normal alveolar septation. D. Histological sections of *Tmem16a*$^{-/-}$ lungs at P0 demonstrate normal prenatal lung development. At E. P3 and F. P21, the lung parenchyma was much thinner in *Tmem16a* mutants and the distal airways were larger, suggesting a failure in the septation of alveoli. Scale bar=50µm.

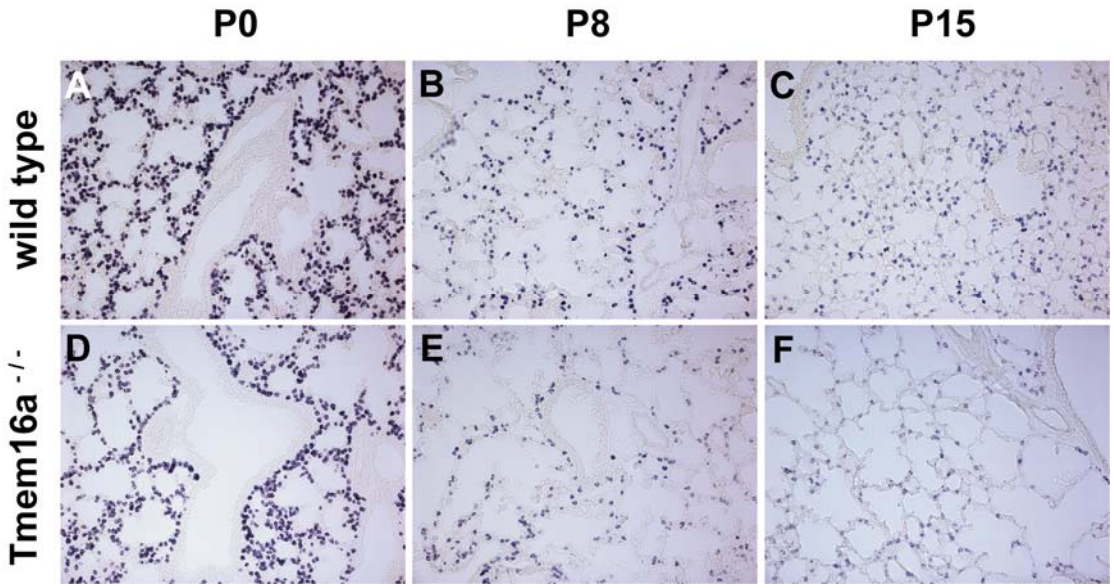

Figure 5-3. Type II alveolar epithelial cells in *Tmem16a* mutant lungs. A-C. RNA *in situ* hybridization using a *Sftpc* probe identifies the normal distribution of type II AECs at A. P0, B. P8, and C. P15. D-F. *Sftpc*-expressing type II AECS are found in the lungs of *Tmem16a* mutants at D. P0, E. P8, and F. P15.

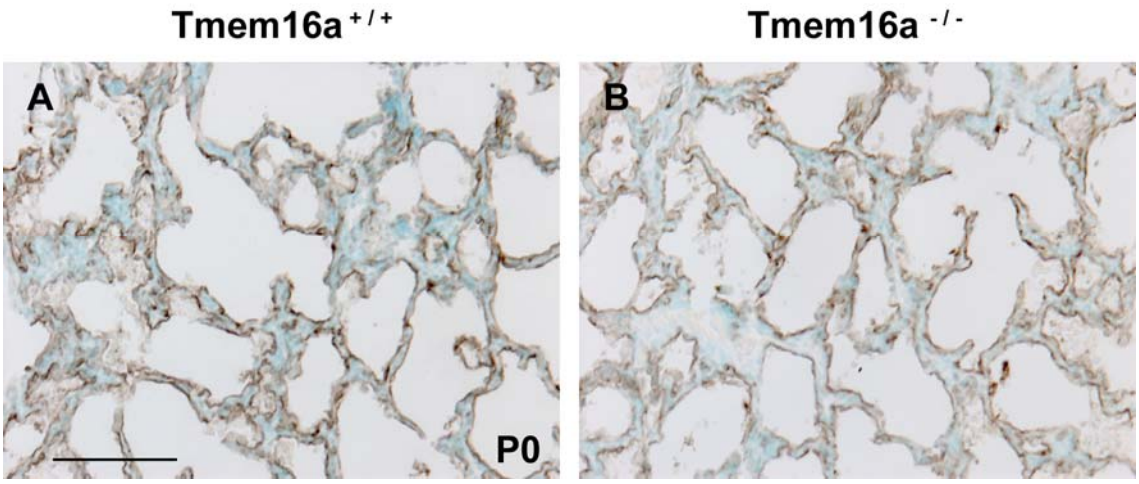

Figure 5-4. Type I alveolar epithelial cells in *Tmem16a* mutant lungs. A. Immunohistochemistry shows the glycoprotein T1α on the membranes of type I AECs in wild type newborn lungs. B. A similar distribution of T1α in *Tmem16a* mutant newborn lungs suggests normal development of type I AECs had occurred. Scale bar=100μm.

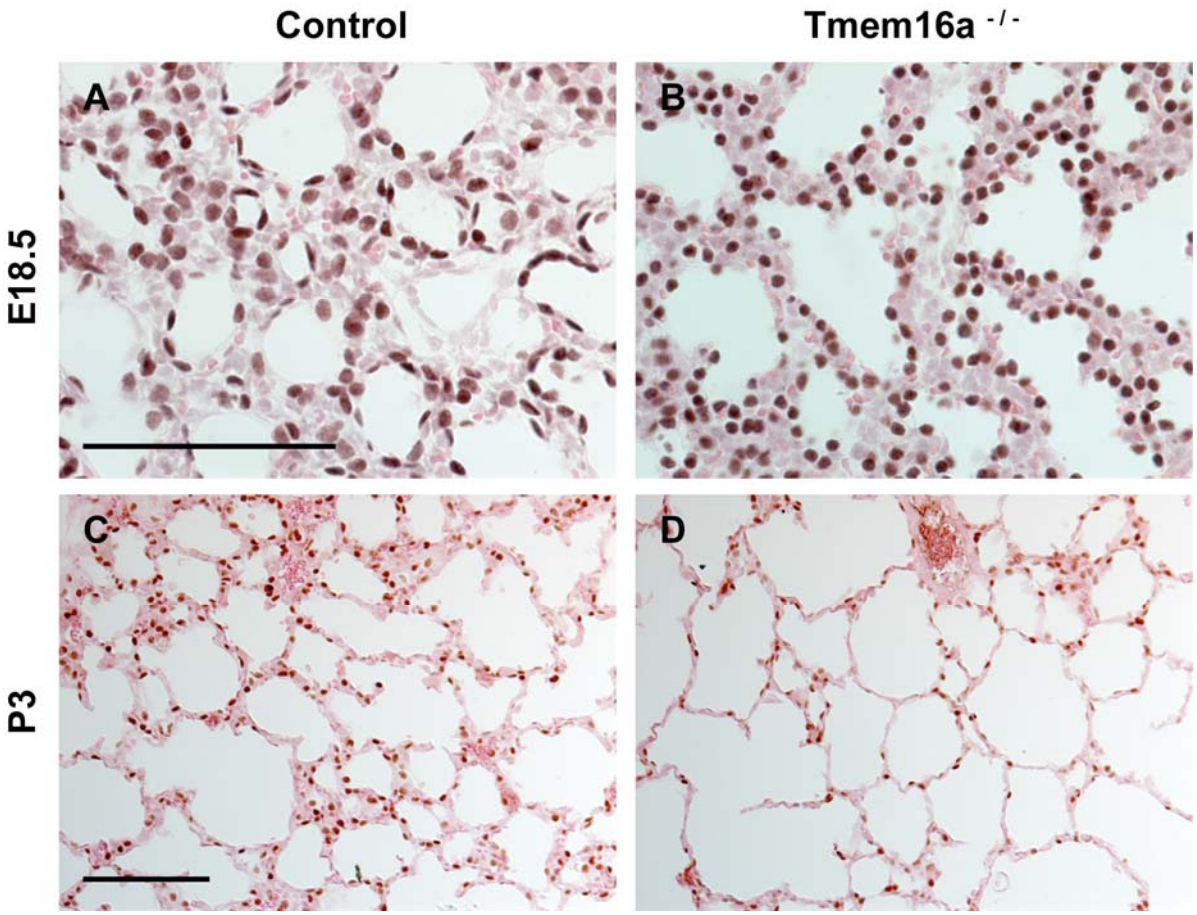

Figure 5-5. Nkx2.1 marks distal epithelial cells in wild type and *Tmem16a* mutant lungs. A. Nkx2.1 immunohistochemistry reveals nuclei of distal epithelial cells in wild type lungs at E18.5. B. Nkx2.1-positive cells have a normal distribution in *Tmem16a* mutant lungs at E18.5. Notice their rounded morphology (see text). C. Nkx2.1-positive cells in wild type lung at P3. D. Nkx2.1-positive cells in *Tmem16a* mutant lung at P3 with distribution similar to that of wild type lung. Notice the enlarged distal airways and the thin parenchyma of the mutant lung. Scale bars=100µm.

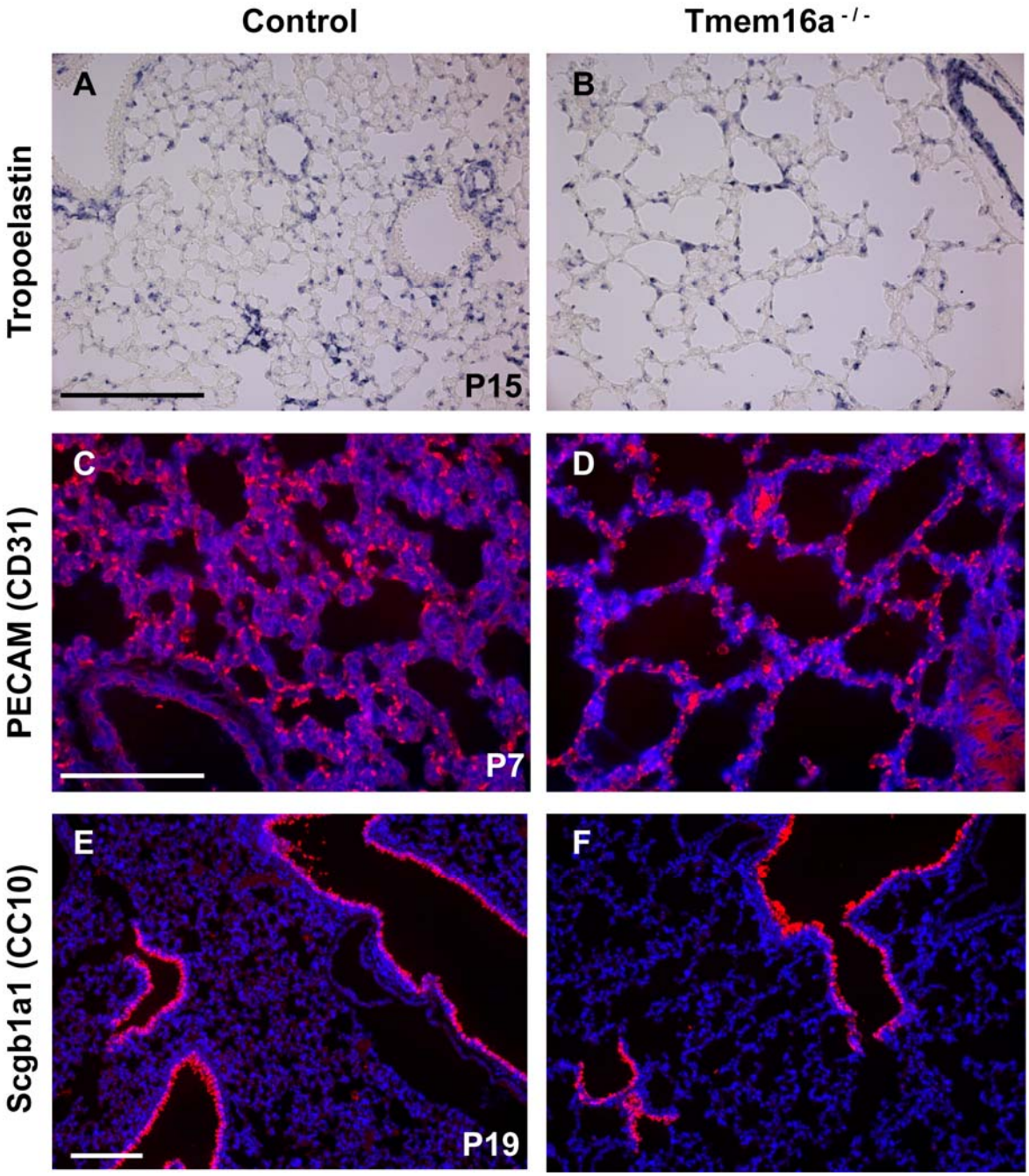

Figure 5-6. Other markers of differentiation in *Tmem16a* mutant lungs. Tropoelastin-expressing myofibroblasts identified by RNA *in situ* hybridization in A. wild type and B. *Tmem16a* mutant lungs at P15. PECAM immunofluorescence revealed the endothelium of the capillary network in C. wild type and D. *Tmem16a* mutant lungs at P7. *Scgb1a1* immunofluorescence revealed Clara cells in the conducting airways of E. wild type and F. *Tmem16a* mutant lungs at P19. Scale bars=200μm.

CHAPTER 6
CONCLUDING REMARKS

By combining two powerful techniques, targeted transgenesis of the mouse genome and microarray technology, we were able to identify six genes expressed in the mouse limb that had not been previously reported (Chapter 2). At least four of these genes are expressed in domains that overlap with the ZPA, but their functions there remain unknown.

To investigate the function of *Tmem16a* in vertebrate development, we generated a null mouse allele of this gene (Chapter 3). *Tmem16a* null mice (as well as mice null for *Tcfap2b* and *Hlxb9*- other genes identified by our screen) did not exhibit patterning defects of the limb. It is possible that this is attributable to compensation by other members of these gene families. In Chapter 4 of this dissertation, we showed that the expression patterns of *Tmem16a* and *Tmem16f* overlapped in a number of developing tissues including the vertebral periostea, the submandibular salivary glands, the muscularis externa of the esophagus, and the lung epithelium. Given the degree of conservation between these proteins (~40% identical at the amino acid level), the mutation of one might be compensated for by the function of another in sites where they are coexpressed. To further characterize the functions of this family in the future, it might be necessary to delete combinations of multiple family members.

We have demonstrated that the mid-gestational epithelium of *Tmem16a* mutant tracheae fails to stratify (see Chapter 3). We currently propose that epithelial cells from which *Tmem16a* has been deleted do not correctly form the cell:cell contacts required to achieve stratification. In support of this hypothesis, transfection of the related family member *TMEM16G* (that localizes to sites of cell:cell contact) into an epithelial cancer cell line alters their morphology and causes aberrant clumps of cells (Tsutsumi et al., 2004). This suggests that members of this family can promote intercellular adhesion. Another possibility is that asymmetric cell divisions that self-

renew the basal layer and generate suprabasal cells required for stratification are aberrant in *Tmem16a* mutant tracheal epithelium (for an example of asymmetric cell divisions in stratification, see (Lechler and Fuchs, 2005)). The single homolog of *Tmem16a* in yeast, *IST2*, has been shown to sort asymmetrically during budding (Takizawa et al., 2000). A final possibility is that deletion of *Tmem16a* interferes with the cytoskeleton of the tracheal epithelium and so cells do not have the proper structural support to achieve stratification. A *Drosophila* homolog, AXS, has been shown to associate with the meiotic spindle (Kramer and Hawley, 2003).

Despite its etiology, the failure of the embryonic tracheal epithelium to stratify in *Tmem16a* mutants causes it to expand and drastically influence the fate of the mesenchymal cells that surround it. Instead of forming a single C-shaped cartilaginous ring, multiple cartilaginous elements form around the trachea of *Tmem16a* mutants. In humans, malformation of the tracheal cartilage is known as tracheomalacia (McNamara and Crabbe, 2004). The symptoms of tracheomalacia worsen during periods of feeding, leading us to speculate that the failure of *Tmem16a* mutants to thrive postnatally is at least partly attributable to the malformation of the cartilage rings.

It is likely that many other defects exist in *Tmem16a* mutants; however, any defect that is observed in the postnatal period will need to be meticulously investigated since these animals fail to thrive and might show signs of generalized distress. The emphysema we characterized in *Tmem16a* mutants might be a secondary defect of this nature. One reagent that will be extremely helpful in the further characterization of *Tmem16a* is a conditional null allele with which an investigator could ablate this gene in a tissue-specific manner. Another reagent that will be necessary to continue this work is an antibody that specifically recognizes and binds murine

TMEM16A. This would allow the subcellular localization of the protein and might provide insights into its function.

The expression of *TMEM16A* in many human cancers, its widespread developmental expression in mice, and the postnatal lethality associated with its deletion in mice suggest that this gene carries significant implications for both the clinic and for basic science. Furthermore, the conservation of TMEM16 orthologs in organisms as distantly related to humans as *S. cerevisiae* indicates that the acquisition of TMEM16 function occurred early in evolutionary history. An integrative approach combining the scant experimental data from all TMEM16 homologs will be required as we attempt to incorporate these molecules into our understanding of development and disease.

APPENDIX A
OLIGONUCLEOTIDES USED AS GENOTYPING PRIMERS

Table A-1. Primers used to genotype *Tmem16a* and *Tmem16f* alleles.

Tmem16a

wild type F: pTKO18F2
5'- CCTATGACTGCCAGGGACGCCC
R: pTKO18R2
5'- TGTTCCTGTCCCTGCAATGCGG

mutant F: pTKOneogenoF
5'- GACGCCCTCCATTGACCC
R: neoR1(Frt)
5'- GGAGTAGAAGGTGGCGCGAAG

Tmem16f (RRF355)

wild type F: Tmem16f ABF2
5'- GTGTAGTTGCTGCATGGTCC
R: wtTMEM16F-R
5'- CAGATCTCATTACAGATGGTTG

mutant F: Tmem16f-F4
5'- GTCACGCTGTGTGCGAGCG
R: En2-R
5'- CGACTTCCGGAGCGGATCTC

APPENDIX B
EXPRESSION OF TMEM16 FAMILY MEMBERS IN CRANIOFACIAL DEVELOPMENT

	Tmem 16a	*Tmem 16c*	*Tmem 16f*	*Tmem 16h*	*Tmem 16k*
Brain					
neuroepithelium	Ventral (+++). Dorsal (+)	(++)	(+++)	(++)	(++)
subventricular layer	(+++)	(+++)	(+++)	(+++)	(-)
differentiating fields	(++)	(+++)	(+++)	(+++)	(+++)
Spinal cord					
neuroepithelium	(+)	(+)	(++)	(+)	(+)
marginal layer	(+)	(+++)	motor neuron area (+++)	(+++)	(+++)
roof plate	(+++) at E12.5	(+)	(+)	(+)	(+)
Eye					
outer retinal cell layers	(+++)	(+)	(+)	(+)	(+)
retinal ganglionic cell layer	(++)	(+++)	(+++)	(+++)	(+++)
lens epithelium	(+++)	(+) at E12.5. Absent at later stages	(-)	(-)	(++) up to E14.5
hyaloid vascular plexus	(+++)	(-)	(+++)	(++)	(+)
ocular mesenchyme	corneal mesenchyme (+++) up to E14.5	(-)	periocular mesenchyme (++)	periocular mesenchyme (+)	periocular mesenchyme (+)
Inner ear					
epithelium	(-)	(-)	(++)	(++)	Before E18.5 (++). After E18.5 (+)
neurosensory patches	(+++)	(-)	similar to the rest of epithelium	similar to the rest of epithelium	similar to the rest of epithelium
organ of Corti	(+++)	(-)	idem above	idem above	idem above
Reissner's membrane	(-)	(-)	(+++)	(+)	(-)
membranous labyrinth	(+)	(-)	(+)	(+)	(-)
stria vascularis	(+++)	(-)	(+++)	(+)	(+)
Pituitary	(+++)	(+)	(+++)	(+++)	(++)
Cranial nerve ganglia	(+++). Also in cells along the trieeminal axons	(+++)	(+++)	(+++)	(+++)
Developing leptomeninges	(+++)	(+)	(+++)	(+)	(++)
Walls of craniofacial vessels	(+++)	(-)	(*)	(*)	(*)
Olfactory epithelium	(+++)Before E18.5.(+) after E18.5	(-)	(++)	(++)	(++)
Olfactory ensheathing cells	(+++)	(-)	(+++)**	(++)**	(+)**
Nasal respiratory epithelium	(+++)	(+)	(+++)	(++)	(++)
Epithelium of the nasal septum	(-) before E14. (+++)after E14	(-)	(++)	(+)	(+)
Tongue					
epithelium	(++)	(-)	(++)	(+)	(+)
mesenchyme	(+++)before E14.5. (+++) nested atE14.5	nested (+++)	(++)	(+)	(++)
lingual vessels	(+++)	(-)	(*)	(*)	(*)
Palate					
shelf epithelium	(++) before E13.5, (+) at E13.5	(+) at E12.5; (-) after E12.5	(++)	(++)	(++)
shelf mesenchyme	(-)	(++) at E12.5. (-) after E12.5	(++)	(++)	(++)
medial edge epithelium	(+) at E13.5 (+++) at E14.5	(-)	(++)	(++)	(++)
medial epithelial seam	(+++)	(-)	(++)	(++)	(++)

	Tmem 16a	*Tmem 16c*	*Tmem 16f*	*Tmem 16h*	*Tmem 16k*
Cartilage					
proliferating chondrocytes	(-)	(+)	(+)	(+)	(++)
prehypertrophic chondrocytes	(+)	(+++)	(++)	(+)	(++)
hypertrophic chondrocytes	(+++)	(+++)	(+++)	(+)	(+)
perichondrium	(+++)	(+)	(+++)	(+)	(+)
Bone					
differentiating osteoblasts	(+++)	(++)	(++)	(+)	(+)
osteoblasts	(+++)	(+++)	(+++)	(+)	(+)
Skin					
epidermis	suprabasal layers (+++)	suprabasal layers (+++)	(++)	(+)	suprabasal layers (+++)
dermis	(+++) at E13.5. (++) at later stages	(+)	(+++)	(+)	(+)
hair follicles	(+)	(-)	(+)	(+)	(+)
Tooth					
early dental epithelium E11.5)	(+)	(+++) nested	(+)	(+)	(+)
early dental mesenchyme (E11.5)	(+++) broad domain	(+++) nested	(+)	(+)	(+)
enamel knot	(-)	(+++)	(+)	(+)	(+)
inner enamel epithelium (IEE)	incisors (+++), (+) molars, (+++) cervical loops	(-)	(-)	(+)	(++)
outer enamel epithelium	(+)	(-)	(-)	(+)	(+)
dental papilla mesenchyme-cap stage	(++)	(+++)	(+)	(+)	(+)
dental papilla mesenchyme - bell stage	(+++) in nasecnt cusps. (+) in developed cusns	(+++)	(++)	Nd	(+++)
dental sac mesenchyme	(+)	(+++) at the cap stage. (-) at later stages	(+)	Nd	(+)
preodontoblasts	(+)	(+++)	(+++)	Nd	(+++)
differentiating odontoblasts	(+++)	(+++)	(+++)	Nd	(+++)
odontoblasts	(++)	(++)	(+)	Nd	(++)
preameloblasts	(+++)	(-)	(++)	Nd	(+)
secretory ameloblasts	(+)	(-)	(+++)	Nd	(+)
maturation stage ameloblasts	(-)	(-)	(+++)	Nd	Nd
stratum intermedium	(+)	(-)	(++)	Nd	(+)
papillary layer	(-)	(-)	(+++)	Nd	Nd
cemetoblasts	(-)	(+++)	(***)	Nd	Nd
periodontal ligament	(-)	(-)	(+++)	Nd	Nd
Salivary glands					
epithelium	(+++)	(+)	(+)	(+)	(+)
mesenchyme	(+)	(+)	(+)	(+)	(+)
submandibular ganglion	(-)	(+++)	(+++)	(-)	(-)

Figure B-1. Summary of *Tmem16a*, *Tmem16c*, *Tmem16f*, *Tmem16h* and *Tmem16k* expression in the nervous system and craniofacial structures. Abbreviations: Virtually absent transcripts (-), expression at slightly above background levels (+), moderate expression levels (++), robust expression levels (+++). Nd, not determined. (*), possible presence of transcripts that may be masked by ubiquitous expression in the core mesenchyme. **, expression in the totality of the connective tissue underlying the olfactory epithelium and thus, may also include the olfactory ensheathing cells. (***), possible expression that may be masked by the signal within the periodontal ligament.

APPENDIX C
PROBES USED FOR RNA *IN SITU* HYBRIDIZATIONS

Table C-1. Probes used for RNA *in situ* hybridizations.

Gene Name	Plasmid Number	Accession Number	Antisense Enzyme	Antisense Polymerase
Tmem16a	BH1	BC006062	SalI	T7
Tmem16c	BH119	BM936471	XhoI	T3
Tmem16f	BH118	BU705523	SalI	T3
*Tmem16h**	BH116	BE571138	SalI	T7
*Tmem16k**	BH117	BF780617	KpnI	T7
Sftpc	BH177		NcoI	SP6
Tropoelastin	BH176		NotI	T3
Shh	BH39		HindIII	T3
*cTmem16a***	BH166	BU248576	NotI	T3

*=probe not used in this dissertation. **=chicken EST (all others are mouse)

LIST OF REFERENCES

Ahel, V., Banac, S., Rozmanic, V., Vukas, D., Drescik, I. and Ahel, V. A., Jr. (2003). Aortopexy and bronchopexy for the management of severe tracheomalacia and bronchomalacia. *Pediatr Int* **45**, 104-6.

Asou, Y., Nifuji, A., Tsuji, K., Shinomiya, K., Olson, E. N., Koopman, P. and Noda, M. (2002). Coordinated expression of scleraxis and Sox9 genes during embryonic development of tendons and cartilage. *J Orthop Res* **20**, 827-33.

Aubin, J., Lemieux, M., Tremblay, M., Berard, J. and Jeannotte, L. (1997). Early postnatal lethality in Hoxa-5 mutant mice is attributable to respiratory tract defects. *Dev Biol* **192**, 432-45.

Bandyopadhyay, A., Tsuji, K., Cox, K., Harfe, B. D., Rosen, V. and Tabin, C. J. (2006). Genetic Analysis of the Roles of BMP2, BMP4, and BMP7 in Limb Patterning and Skeletogenesis. *PLoS Genet* **2**, e216.

Bera, T. K., Das, S., Maeda, H., Beers, R., Wolfgang, C. D., Kumar, V., Hahn, Y., Lee, B. and Pastan, I. (2004). NGEP, a gene encoding a membrane protein detected only in prostate cancer and normal prostate. *Proc Natl Acad Sci U S A* **101**, 3059-64.

Berthiaume, Y., Voisin, G. and Dagenais, A. (2006). The alveolar type I cells: the new knight of the alveolus? *J Physiol* **572**, 609-10.

Bhaskaran, M., Kolliputi, N., Wang, Y., Gou, D., Chintagari, N. R. and Liu, L. (2007). Trans-differentiation of alveolar epithelial type II cells to type I cells involves autocrine signaling by transforming growth factor beta 1 through the Smad pathway. *J Biol Chem* **282**, 3968-76.

Boogaard, R., Huijsmans, S. H., Pijnenburg, M. W., Tiddens, H. A., de Jongste, J. C. and Merkus, P. J. (2005). Tracheomalacia and bronchomalacia in children: incidence and patient characteristics. *Chest* **128**, 3391-7.

Boulet, A. M., Moon, A. M., Arenkiel, B. R. and Capecchi, M. R. (2004). The roles of Fgf4 and Fgf8 in limb bud initiation and outgrowth. *Dev Biol* **273**, 361-72.

Burri, P. H. (2006). Structural aspects of postnatal lung development - alveolar formation and growth. *Biol Neonate* **89**, 313-22.

Carden, K. A., Boiselle, P. M., Waltz, D. A. and Ernst, A. (2005). Tracheomalacia and tracheobronchomalacia in children and adults: an in-depth review. *Chest* **127**, 984-1005.

Cardoso, W. V. and Lu, J. (2006). Regulation of early lung morphogenesis: questions, facts and controversies. *Development* **133**, 1611-24.

Chan, A. S., Thorner, P. S., Squire, J. A. and Zielenska, M. (2002). Identification of a novel gene NCRMS on chromosome 12q21 with differential expression between rhabdomyosarcoma subtypes. *Oncogene* **21**, 3029-37.

Chiang, C., Litingtung, Y., Lee, E., Young, K. E., Corden, J. L., Westphal, H. and Beachy, P. A. (1996). Cyclopia and defective axial patterning in mice lacking Sonic hedgehog gene function. *Nature* **383**, 407-13.

Cillo, C., Cantile, M., Faiella, A. and Boncinelli, E. (2001). Homeobox genes in normal and malignant cells. *J Cell Physiol* **188**, 161-9.

Daniely, Y., Liao, G., Dixon, D., Linnoila, R. I., Lori, A., Randell, S. H., Oren, M. and Jetten, A. M. (2004). Critical role of p63 in the development of a normal esophageal and tracheobronchial epithelium. *Am J Physiol Cell Physiol* **287**, C171-81.

Das, S., Hahn, Y., Nagata, S., Willingham, M. C., Bera, T. K., Lee, B. and Pastan, I. (2007). NGEP, a prostate-specific plasma membrane protein that promotes the association of LNCaP cells. *Cancer Res* **67**, 1594-601.

de Crombrugghe, B., Lefebvre, V. and Nakashima, K. (2001). Regulatory mechanisms in the pathways of cartilage and bone formation. *Curr Opin Cell Biol* **13**, 721-7.

Eblaghie, M. C., Reedy, M., Oliver, T., Mishina, Y. and Hogan, B. L. (2006). Evidence that autocrine signaling through Bmpr1a regulates the proliferation, survival and morphogenetic behavior of distal lung epithelial cells. *Dev Biol* **291**, 67-82.

Echelard, Y., Epstein, D. J., St-Jacques, B., Shen, L., Mohler, J., McMahon, J. A. and McMahon, A. P. (1993). Sonic hedgehog, a member of a family of putative signaling molecules, is implicated in the regulation of CNS polarity. *Cell* **75**, 1417-30.

Elluru, R. G. and Whitsett, J. A. (2004). Potential role of Sox9 in patterning tracheal cartilage ring formation in an embryonic mouse model. *Arch Otolaryngol Head Neck Surg* **130**, 732-6.

Entian, K. D., Schuster, T., Hegemann, J. H., Becher, D., Feldmann, H., Guldener, U., Gotz, R., Hansen, M., Hollenberg, C. P., Jansen, G. et al. (1999). Functional analysis of 150 deletion mutants in Saccharomyces cerevisiae by a systematic approach. *Mol Gen Genet* **262**, 683-702.

Espinosa, I., Lee, C. H., Kim, M. K., Rouse, B. T., Subramanian, S., Montgomery, K., Varma, S., Corless, C. L., Heinrich, M. C., Smith, K. S. et al. (2008). A Novel Monoclonal Antibody Against DOG1 is a Sensitive and Specific Marker for Gastrointestinal Stromal Tumors. *Am J Surg Pathol* **32**, 210-218.

Evans, M. J., Cabral, L. J., Stephens, R. J. and Freeman, G. (1975). Transformation of alveolar type 2 cells to type 1 cells following exposure to NO2. *Exp Mol Pathol* **22**, 142-50.

Fehrenbach, H. (2001). Alveolar epithelial type II cell: defender of the alveolus revisited. *Respir Res* **2**, 33-46.

Galindo, B. E. and Vacquier, V. D. (2005). Phylogeny of the TMEM16 protein family: some members are overexpressed in cancer. *Int J Mol Med* **16**, 919-24.

Ganan, Y., Macias, D., Basco, R. D., Merino, R. and Hurle, J. M. (1998). Morphological diversity of the avian foot is related with the pattern of msx gene expression in the developing autopod. *Dev Biol* **196**, 33-41.

Gomperts, B. N., Gong-Cooper, X. and Hackett, B. P. (2004). Foxj1 regulates basal body anchoring to the cytoskeleton of ciliated pulmonary epithelial cells. *J Cell Sci* **117**, 1329-37.

Greenholz, S. K., Karrer, F. M. and Lilly, J. R. (1986). Contemporary surgery of tracheomalacia. *J Pediatr Surg* **21**, 511-4.

Harfe, B. D., Scherz, P. J., Nissim, S., Tian, H., McMahon, A. P. and Tabin, C. J. (2004). Evidence for an expansion-based temporal Shh gradient in specifying vertebrate digit identities. *Cell* **118**, 517-28.

Harrison, K. A., Thaler, J., Pfaff, S. L., Gu, H. and Kehrl, J. H. (1999). Pancreas dorsal lobe agenesis and abnormal islets of Langerhans in Hlxb9-deficient mice. *Nat Genet* **23**, 71-5.

Hecht, J., Seitz, V., Urban, M., Wagner, F., Robinson, P. N., Stiege, A., Dieterich, C., Kornak, U., Wilkening, U., Brieske, N. et al. (2007). Detection of novel skeletogenesis target genes by comprehensive analysis of a Runx2(-/-) mouse model. *Gene Expr Patterns* **7**, 102-12.

Hogan, B. L. (1996). Bone morphogenetic proteins: multifunctional regulators of vertebrate development. *Genes Dev* **10**, 1580-94.

Hong, K. U., Reynolds, S. D., Watkins, S., Fuchs, E. and Stripp, B. R. (2004). In vivo differentiation potential of tracheal basal cells: evidence for multipotent and unipotent subpopulations. *Am J Physiol Lung Cell Mol Physiol* **286**, L643-9.

Huang, T., You, Y., Spoor, M. S., Richer, E. J., Kudva, V. V., Paige, R. C., Seiler, M. P., Liebler, J. M., Zabner, J., Plopper, C. G. et al. (2003). Foxj1 is required for apical localization of ezrin in airway epithelial cells. *J Cell Sci* **116**, 4935-45.

Huang, X., Godfrey, T. E., Gooding, W. E., McCarty, K. S., Jr. and Gollin, S. M. (2006). Comprehensive genome and transcriptome analysis of the 11q13 amplicon in human oral cancer and synteny to the 7F5 amplicon in murine oral carcinoma. *Genes Chromosomes Cancer* **45**, 1058-69.

Kalenga, M. (1997). Lung growth and development during experimental malnutrition. *Pediatr Pulmonol Suppl* **16**, 165-6.

Katoh, M. and Katoh, M. (2003). FLJ10261 gene, located within the CCND1-EMS1 locus on human chromosome 11q13, encodes the eight-transmembrane protein homologous to C12orf3, C11orf25 and FLJ34272 gene products. *Int J Oncol* **22**, 1375-81.

Katoh, M. and Katoh, M. (2005). Identification and characterization of TMEM16H gene in silico. *Int J Mol Med* **15**, 353-8.

Kiessling, A., Weigle, B., Fuessel, S., Ebner, R., Meye, A., Rieger, M. A., Schmitz, M., Temme, A., Bachmann, M., Wirth, M. P. et al. (2005). D-TMPP: a novel androgen-regulated gene preferentially expressed in prostate and prostate cancer that is the first characterized member of an eukaryotic gene family. *Prostate* **64**, 387-400.

Kramer, J. and Hawley, R. S. (2003). The spindle-associated transmembrane protein Axs identifies a new family of transmembrane proteins in eukaryotes. *Cell Cycle* **2**, 174-6.

Laufer, E., Nelson, C. E., Johnson, R. L., Morgan, B. A. and Tabin, C. (1994). Sonic hedgehog and Fgf-4 act through a signaling cascade and feedback loop to integrate growth and patterning of the developing limb bud. *Cell* **79**, 993-1003.

Lechler, T. and Fuchs, E. (2005). Asymmetric cell divisions promote stratification and differentiation of mammalian skin. *Nature* **437**, 275-80.

Lefebvre, V., Huang, W., Harley, V. R., Goodfellow, P. N. and de Crombrugghe, B. (1997). SOX9 is a potent activator of the chondrocyte-specific enhancer of the pro alpha1(II) collagen gene. *Mol Cell Biol* **17**, 2336-46.

Lettice, L. A., Heaney, S. J., Purdie, L. A., Li, L., de Beer, P., Oostra, B. A., Goode, D., Elgar, G., Hill, R. E. and de Graaff, E. (2003). A long-range Shh enhancer regulates expression in the developing limb and fin and is associated with preaxial polydactyly. *Hum Mol Genet* **12**, 1725-35.

Lindahl, P., Karlsson, L., Hellstrom, M., Gebre-Medhin, S., Willetts, K., Heath, J. K. and Betsholtz, C. (1997). Alveogenesis failure in PDGF-A-deficient mice is coupled to lack of distal spreading of alveolar smooth muscle cell progenitors during lung development. *Development* **124**, 3943-53.

Liu, W., Selever, J., Wang, D., Lu, M. F., Moses, K. A., Schwartz, R. J. and Martin, J. F. (2004). Bmp4 signaling is required for outflow-tract septation and branchial-arch artery remodeling. *Proc Natl Acad Sci U S A* **101**, 4489-94.

Logan, M., Martin, J. F., Nagy, A., Lobe, C., Olson, E. N. and Tabin, C. J. (2002). Expression of Cre Recombinase in the developing mouse limb bud driven by a Prxl enhancer. *Genesis* **33**, 77-80.

Mahlapuu, M., Enerback, S. and Carlsson, P. (2001). Haploinsufficiency of the forkhead gene Foxf1, a target for sonic hedgehog signaling, causes lung and foregut malformations. *Development* **128**, 2397-406.

Manak, J. R. and Scott, M. P. (1994). A class act: conservation of homeodomain protein functions. *Dev Suppl*, 61-77.

Massaro, D., Massaro, G. D., Baras, A., Hoffman, E. P. and Clerch, L. B. (2004). Calorie-related rapid onset of alveolar loss, regeneration, and changes in mouse lung gene expression. *Am J Physiol Lung Cell Mol Physiol* **286**, L896-906.

McNamara, V. M. and Crabbe, D. C. (2004). Tracheomalacia. *Paediatr Respir Rev* **5**, 147-54.

Mendelsohn, C., Lohnes, D., Decimo, D., Lufkin, T., LeMeur, M., Chambon, P. and Mark, M. (1994). Function of the retinoic acid receptors (RARs) during development (II). Multiple abnormalities at various stages of organogenesis in RAR double mutants. *Development* **120**, 2749-71.

Miller, L. A., Wert, S. E., Clark, J. C., Xu, Y., Perl, A. K. and Whitsett, J. A. (2004). Role of Sonic hedgehog in patterning of tracheal-bronchial cartilage and the peripheral lung. *Dev Dyn* **231**, 57-71.

Minoo, P., Su, G., Drum, H., Bringas, P. and Kimura, S. (1999). Defects in tracheoesophageal and lung morphogenesis in Nkx2.1(-/-) mouse embryos. *Dev Biol* **209**, 60-71.

Mizuta, K., Tsutsumi, S., Inoue, H., Sakamoto, Y., Miyatake, K., Miyawaki, K., Noji, S., Kamata, N. and Itakura, M. (2007). Molecular characterization of GDD1/TMEM16E, the gene product responsible for autosomal dominant gnathodiaphyseal dysplasia. *Biochem Biophys Res Commun* **357**, 126-32.

Moser, M., Pscherer, A., Roth, C., Becker, J., Mucher, G., Zerres, K., Dixkens, C., Weis, J., Guay-Woodford, L., Buettner, R. et al. (1997a). Enhanced apoptotic cell death of renal epithelial cells in mice lacking transcription factor AP-2beta. *Genes Dev* **11**, 1938-48.

Moser, M., Ruschoff, J. and Buettner, R. (1997b). Comparative analysis of AP-2 alpha and AP-2 beta gene expression during murine embryogenesis. *Dev Dyn* **208**, 115-24.

Nielsen, T. O., West, R. B., Linn, S. C., Alter, O., Knowling, M. A., O'Connell, J. X., Zhu, S., Fero, M., Sherlock, G., Pollack, J. R. et al. (2002). Molecular characterisation of soft tissue tumours: a gene expression study. *Lancet* **359**, 1301-7.

Nieto, M. A., Patel, K. and Wilkinson, D. G. (1996). In situ hybridization analysis of chick embryos in whole mount and tissue sections. *Methods Cell Biol* **51**, 219-35.

Nissim, S., Hasso, S. M., Fallon, J. F. and Tabin, C. J. (2006). Regulation of Gremlin expression in the posterior limb bud. *Dev Biol* **299**, 12-21.

Niswander, L., Jeffrey, S., Martin, G. R. and Tickle, C. (1994). A positive feedback loop coordinates growth and patterning in the vertebrate limb. *Nature* **371**, 609-12.

Noji, S., Nohno, T., Koyama, E., Muto, K., Ohyama, K., Aoki, Y., Tamura, K., Ohsugi, K., Ide, H., Taniguchi, S. et al. (1991). Retinoic acid induces polarizing activity but is unlikely to be a morphogen in the chick limb bud. *Nature* **350**, 80-6.

Perl, A. K., Wert, S. E., Loudy, D. E., Shan, Z., Blair, P. A. and Whitsett, J. A. (2005). Conditional recombination reveals distinct subsets of epithelial cells in trachea, bronchi, and alveoli. *Am J Respir Cell Mol Biol* **33**, 455-62.

Perl, A. K., Wert, S. E., Nagy, A., Lobe, C. G. and Whitsett, J. A. (2002). Early restriction of peripheral and proximal cell lineages during formation of the lung. *Proc Natl Acad Sci U S A* **99**, 10482-7.

Prodhan, P. and Kinane, T. B. (2002). Developmental paradigms in terminal lung development. *Bioessays* **24**, 1052-9.

Provot, S. and Schipani, E. (2005). Molecular mechanisms of endochondral bone development. *Biochem Biophys Res Commun* **328**, 658-65.

Puschel, A. W. (1999). Divergent properties of mouse netrins. *Mech Dev* **83**, 65-75.

Que, J., Choi, M., Ziel, J. W., Klingensmith, J. and Hogan, B. L. (2006). Morphogenesis of the trachea and esophagus: current players and new roles for noggin and Bmps. *Differentiation* **74**, 422-37.

Rawlins, E. L. and Hogan, B. L. (2006). Epithelial stem cells of the lung: privileged few or opportunities for many? *Development* **133**, 2455-65.

Regnier, C. H., Masson, R., Kedinger, V., Textoris, J., Stoll, I., Chenard, M. P., Dierich, A., Tomasetto, C. and Rio, M. C. (2002). Impaired neural tube closure, axial skeleton malformations, and tracheal ring disruption in TRAF4-deficient mice. *Proc Natl Acad Sci U S A* **99**, 5585-90.

Riddle, R. D., Johnson, R. L., Laufer, E. and Tabin, C. (1993). Sonic hedgehog mediates the polarizing activity of the ZPA. *Cell* **75**, 1401-16.

Rock, J. R., Lopez, M. C., Baker, H. V. and Harfe, B. D. (2007). Identification of genes expressed in the mouse limb using a novel ZPA microarray approach. *Gene Expr Patterns* **8**, 19-26.

Samuel, S. and Naora, H. (2005). Homeobox gene expression in cancer: insights from developmental regulation and deregulation. *Eur J Cancer* **41**, 2428-37.

Saunders JW, J. (1948). The proximo-distal sequence of the origin of the parts of the chick wing and the role of the ectoderm. *The Journal of Experimental Zoology* **108**, 363-403.

Saunders JW, J. and Gasseling, MT. (1968). Ectodermal-mesodermal interactions in the origin of limb symmetry. In *Epithelial-Mesenchymal Interactions,* (ed. F. R and B. RE), pp. 78-97. Baltimore: Willilams &Wilkins.

Scherz, P. J., Harfe, B. D., McMahon, A. P. and Tabin, C. J. (2004). The limb bud Shh-Fgf feedback loop is terminated by expansion of former ZPA cells. *Science* **305**, 396-9.

Schuuring, E. (1995). The involvement of the chromosome 11q13 region in human malignancies: cyclin D1 and EMS1 are two new candidate oncogenes--a review. *Gene* **159**, 83-96.

Sekiya, I., Tsuji, K., Koopman, P., Watanabe, H., Yamada, Y., Shinomiya, K., Nifuji, A. and Noda, M. (2000). SOX9 enhances aggrecan gene promoter/enhancer activity and is up-regulated by retinoic acid in a cartilage-derived cell line, TC6. *J Biol Chem* **275**, 10738-44.

Soriano, P. (1999). Generalized lacZ expression with the ROSA26 Cre reporter strain. *Nat Genet* **21**, 70-1.

Sun, X., Mariani, F. V. and Martin, G. R. (2002). Functions of FGF signalling from the apical ectodermal ridge in limb development. *Nature* **418**, 501-8.

Swiatek, P. J. and Gridley, T. (1993). Perinatal lethality and defects in hindbrain development in mice homozygous for a targeted mutation of the zinc finger gene Krox20. *Genes Dev* **7**, 2071-84.

Takizawa, P. A., DeRisi, J. L., Wilhelm, J. E. and Vale, R. D. (2000). Plasma membrane compartmentalization in yeast by messenger RNA transport and a septin diffusion barrier. *Science* **290**, 341-4.

Thaler, J., Harrison, K., Sharma, K., Lettieri, K., Kehrl, J. and Pfaff, S. L. (1999). Active suppression of interneuron programs within developing motor neurons revealed by analysis of homeodomain factor HB9. *Neuron* **23**, 675-87.

Tickle, C., Alberts, B., Wolpert, L. and Lee, J. (1982). Local application of retinoic acid to the limb bud mimics the action of the polarizing region. *Nature* **296**, 564-6.

Tickle, C., Lee, J. and Eichele, G. (1985). A quantitative analysis of the effect of all-trans-retinoic acid on the pattern of chick wing development. *Dev Biol* **109**, 82-95.

Tsuji, K., Bandyopadhyay, A., Harfe, B. D., Cox, K., Kakar, S., Gerstenfeld, L., Einhorn, T., Tabin, C. J. and Rosen, V. (2006). BMP2 activity, although dispensable for bone formation, is required for the initiation of fracture healing. *Nat Genet* **38**, 1424-9.

Tsutsumi, S., Inoue, H., Sakamoto, Y., Mizuta, K., Kamata, N. and Itakura, M. (2005). Molecular cloning and characterization of the murine gnathodiaphyseal dysplasia gene GDD1. *Biochem Biophys Res Commun* **331**, 1099-106.

Tsutsumi, S., Kamata, N., Vokes, T. J., Maruoka, Y., Nakakuki, K., Enomoto, S., Omura, K., Amagasa, T., Nagayama, M., Saito-Ohara, F. et al. (2004). The novel gene encoding a putative transmembrane protein is mutated in gnathodiaphyseal dysplasia (GDD). *Am J Hum Genet* **74**, 1255-61.

Vermot, J., Niederreither, K., Garnier, J. M., Chambon, P. and Dolle, P. (2003). Decreased embryonic retinoic acid synthesis results in a DiGeorge syndrome phenotype in newborn mice. *Proc Natl Acad Sci U S A* **100**, 1763-8.

Wanek, N., Gardiner, D. M., Muneoka, K. and Bryant, S. V. (1991). Conversion by retinoic acid of anterior cells into ZPA cells in the chick wing bud. *Nature* **350**, 81-3.

Warburton, D., Schwarz, M., Tefft, D., Flores-Delgado, G., Anderson, K. D. and Cardoso, W. V. (2000). The molecular basis of lung morphogenesis. *Mech Dev* **92**, 55-81.

Warburton, D., Wuenschell, C., Flores-Delgado, G. and Anderson, K. (1998). Commitment and differentiation of lung cell lineages. *Biochem Cell Biol* **76**, 971-95.

West, R. B., Corless, C. L., Chen, X., Rubin, B. P., Subramanian, S., Montgomery, K., Zhu, S., Ball, C. A., Nielsen, T. O., Patel, R. et al. (2004). The novel marker, DOG1, is expressed ubiquitously in gastrointestinal stromal tumors irrespective of KIT or PDGFRA mutation status. *Am J Pathol* **165**, 107-13.

Wilkinson, D. (1992). Whole mount in situ hybridization to vertebrate embryos. In *Situ Hybridization: A Practical Approach*, (ed. D. Wilkinson), pp. 75-83. Oxford: IRL Press.

Wolpert, L. (1969). Positional information and the spatial pattern of cellular differentiation. *J Theor Biol* **25**, 1-47.

Zuniga, A., Haramis, A. P., McMahon, A. P. and Zeller, R. (1999). Signal relay by BMP antagonism controls the SHH/FGF4 feedback loop in vertebrate limb buds. *Nature* **401**, 598-602.

BIOGRAPHICAL SKETCH

Jason Randall Rock was born March 19, 1981 in Tallahassee, Florida to parents Harry and Glenda Rock. His sister, Sandra, and he were raised in Jacksonville, FL with the exception of two years spent in Knoxville, TN.

From an early age, Jason was extremely interested in science, math, and music. During middle and high school, he participated in activities including Odyssey of the Mind, Science Olympiad, and Brain Brawl. In 1999, Jason received an International Baccalaureate diploma from Stanton College Preparatory High School in Jacksonville, FL.

Jason graduated *magna cum laude* with a Bachelor of Science from the Florida State University in 2002. As an undergraduate student, he performed a directed individual study under the tutelage of Dr. Dexter Easton with whom he also instructed an experimental physiology course. These experiences were instrumental in Jason's decision to pursue a career in academic research. During this time, his interest in natural history and education were exercised as an educator at the Tallahassee Museum of History and Natural Science.

In August of 2003, Jason entered the Interdisciplinary Program in Biomedical Sciences in the College of Medicine at the University of Florida. During the course of laboratory rotations, he developed an intense interest in developmental genetics and became the first graduate student in the laboratory of Dr. Brian Harfe. Following graduation, Jason will join the lab of Dr. Brigid Hogan at Duke University as a postdoctoral associate.